Supplement of Atmos. Chem. Phys., 23, 6217–6240, 2023
https://doi.org/10.5194/acp-23-6217-2023-supplement

Atmospheric Chemistry and Physics
Open Access

Supplement of

Unbalanced emission reductions of different species and sectors in China during COVID-19 lockdown derived by multi-species surface observation assimilation

Lei Kong et al.

Correspondence to: Xiao Tang (tangxiao@mail.iap.ac.cn)

Supplementary Material

Text S1: Evaluation of meteorological simulation

Performance of meteorological simulation is important for the inversion estimation since the meteorological parameters determine the transport process from the sources to the observation and influence the estimation of flow-dependent background error covariance. The air temperature, relative humidity and precipitation also affect the atmospheric chemistry and the removal of air pollutants. The meteorology simulation was evaluated against the daily observations from China Meteorological Administration (CMA) with spatial distribution of meteorological observation sites shown in Fig. S25. Figure S26–31 present the comparisons of simulated and observed regional mean daily meteorological parameters (i.e., u-wind, v-wind, temperature, relatively humidity and precipitation) over six regions of China from January to February 2020, with calculated evaluation statistics summarised in Table S4. In general, the simulation can well capture the main feathers of the observed meteorological conditions in all regions for our simulation period. All variables exhibited small RMSE values in all regions, that are around 1 m/s for wind speed, 1℃ for T, 10% for RH and 0.08–2.38mm for precipitation. Therefore, the WRF can generally well reproduce the meteorological conditions for all regions of China, which is adequate for our inversion estimates.

Text S2: Assessment of the influence of chemiluminescence monitor interference on the inversion of NO_x emission

The NO_2 measurement from CNEMC is made by the chemiluminescent analyser with a molybdenum converter, which is subject to the positive bias induced by the interference of HNO_3, PAN and alkyl nitrates (AN) (Dunlea et al., 2007; Lamsal et al., 2008).To investigate the influence of the chemiluminescence monitor interference on the NO_2 measurement and its impact on the inversion of NO_x emissions, a sensitivity inversion run was conducted based on the corrected NO_2 measurement using the corrected factors (Eq. (1)) proposed by Lamsal et al. (2008). In order to alleviate the effects of emission uncertainty on the CF calculations, the CF values were calculated based on the simulated NO_2, HNO_3, PAN and AN using the inversed emission inventory. Figure S16 shows the calculated CFs for NO_2 measurements over different regions of China during COVID-19 pandemic, which ranged from 0.75 to 0.99. The CF values over NCP, NE, NW and Central were stable throughout the COVID-19 pandemic, all larger than 0.9, suggesting that chemiluminescence monitor interference only has slight effects on the NO_2 measurement there. Over the SE and SW regions, there was a drop of CF values during the lockdown period, followed by an increase after the lockdown, suggesting that the decline of NO_2 concentrations during lockdown period may be larger.

As shown in Figure S17, the overestimations were lower than 3 $\mu g/m^3$ over different regions of China throughout the COVID-19 pandemic, which is smaller than the observation errors (~10 $\mu g/m^3$) we used in the assimilation, suggesting that the observation error caused by the chemiluminescence monitor interference were well considered in our assimilation. To better quantify the influences of chemiluminescence monitor interference on the inversed NO_x emission, an additional inversion experiment was conducted based on the corrected NO_2 measurement using the calculated CFs. The results suggest the chemiluminescence monitor interference in the NO_2 observations had weak impacts on the inversed NO_x emissions as seen in Fig. S18 and Fig. S19, which display the comparisons of the inversed NO_x emission with and without correction in respect of the magnitude and change ratio during different stage of COVID-19 pandemic. The differences in the magnitude of inversed NO_x emissions caused by correction were about 2–7% over the NCP, NE, NW and Central, and were about 10–13% over the SE and SW. The differences in the emission reductions of NO_x were also small, which

was about 0.3 to 4.1 percentage points. These results indicate that due to the considerations of observation error in the EnKF, the chemiluminescence monitor interference to the NO_2 measurement might not significantly influence our inversion results in this application. However, the NO_x emissions could be slightly overestimated due to the positive biases in the NO_2 measurement, and the inversed NO_x emissions may drop faster if the NO_2 measurement was corrected.

Figures

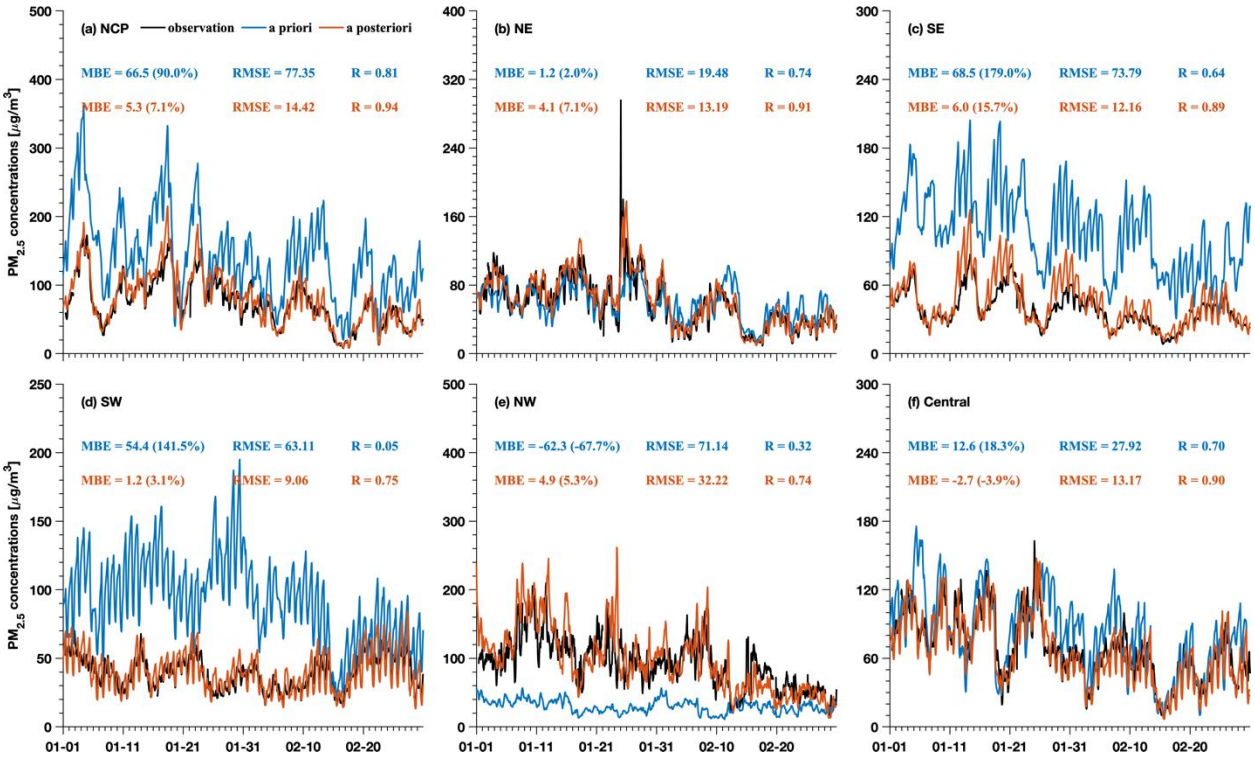

Figure S1: Time series of $PM_{2.5}$ concentrations over (a) NCP, (b) NE, (c) SE, (d) SW, (e) NW and (f) Central regions from 1st Jan to 29th Feb 2020 obtained from observation (black line) and simulation using a priori (blue line) and a posteriori (orange line) emissions.

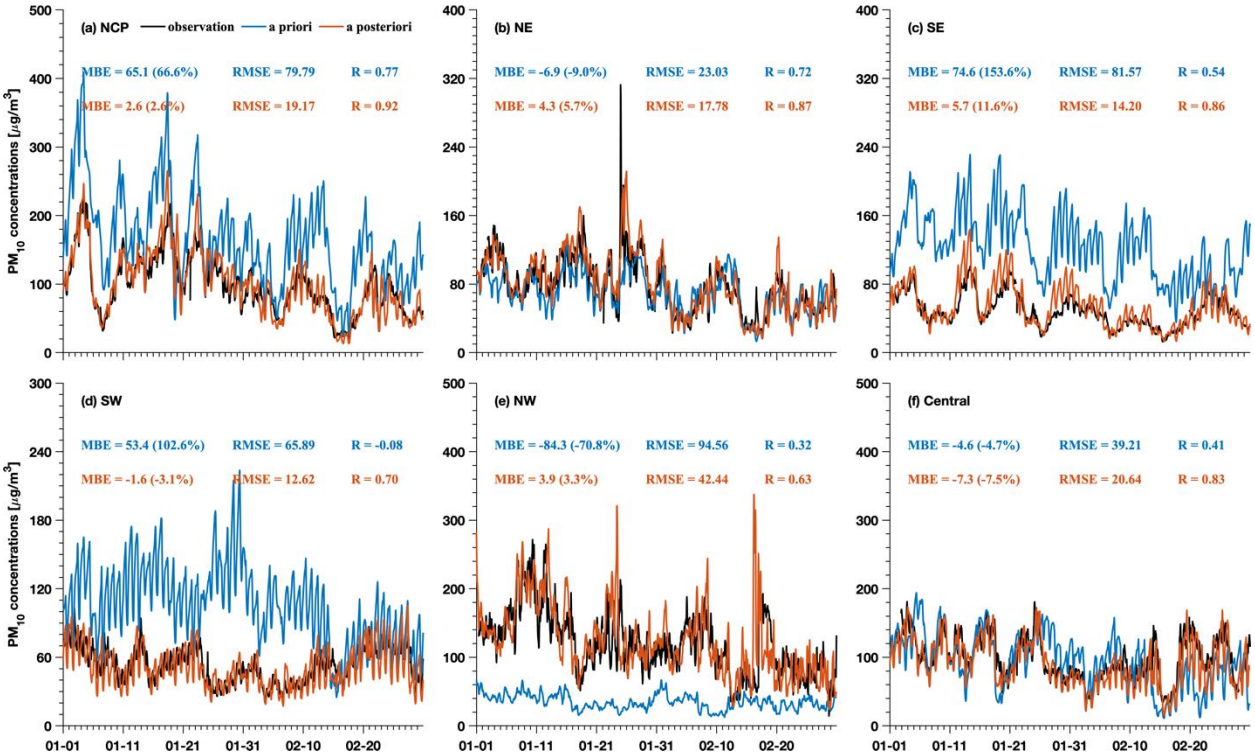

Figure S2: Same as in Fig. S1 but for PM_{10} concentrations.

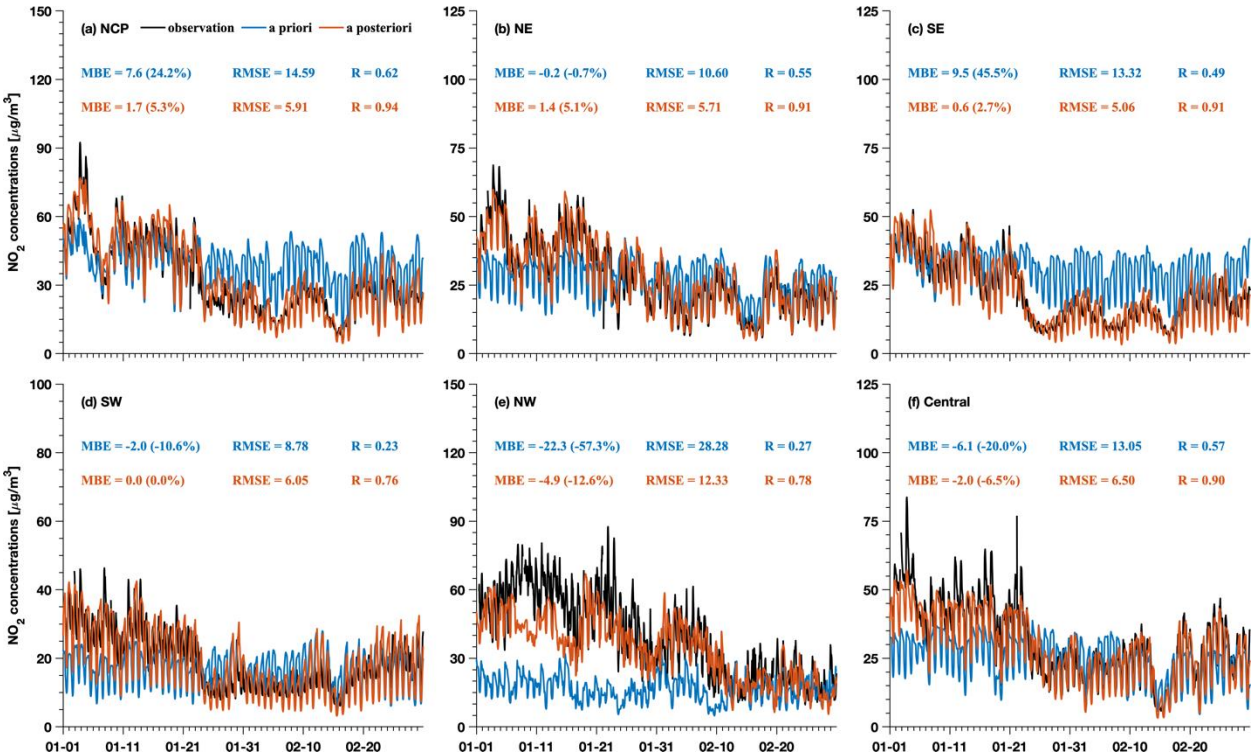

Figure S3: Same as in Fig. S1 but for NO_2 concentrations.

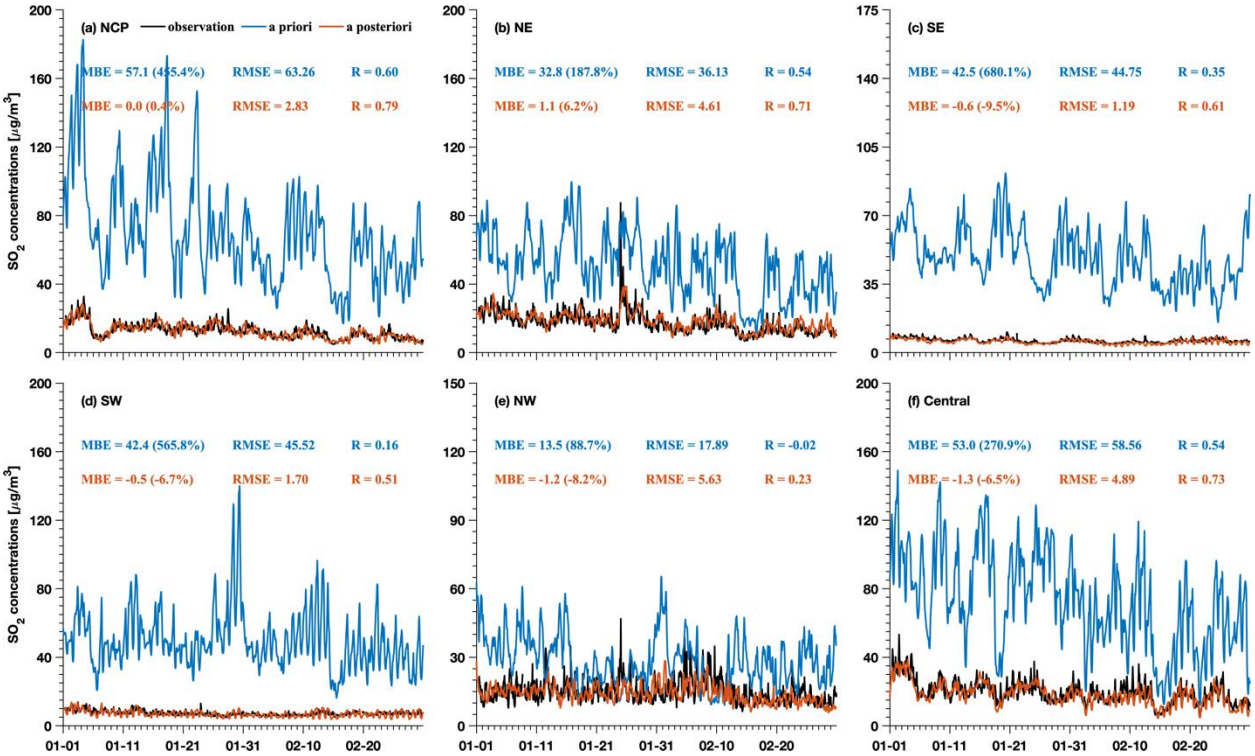

Figure S4: Same as in Fig. S1 but for SO_2 concentrations.

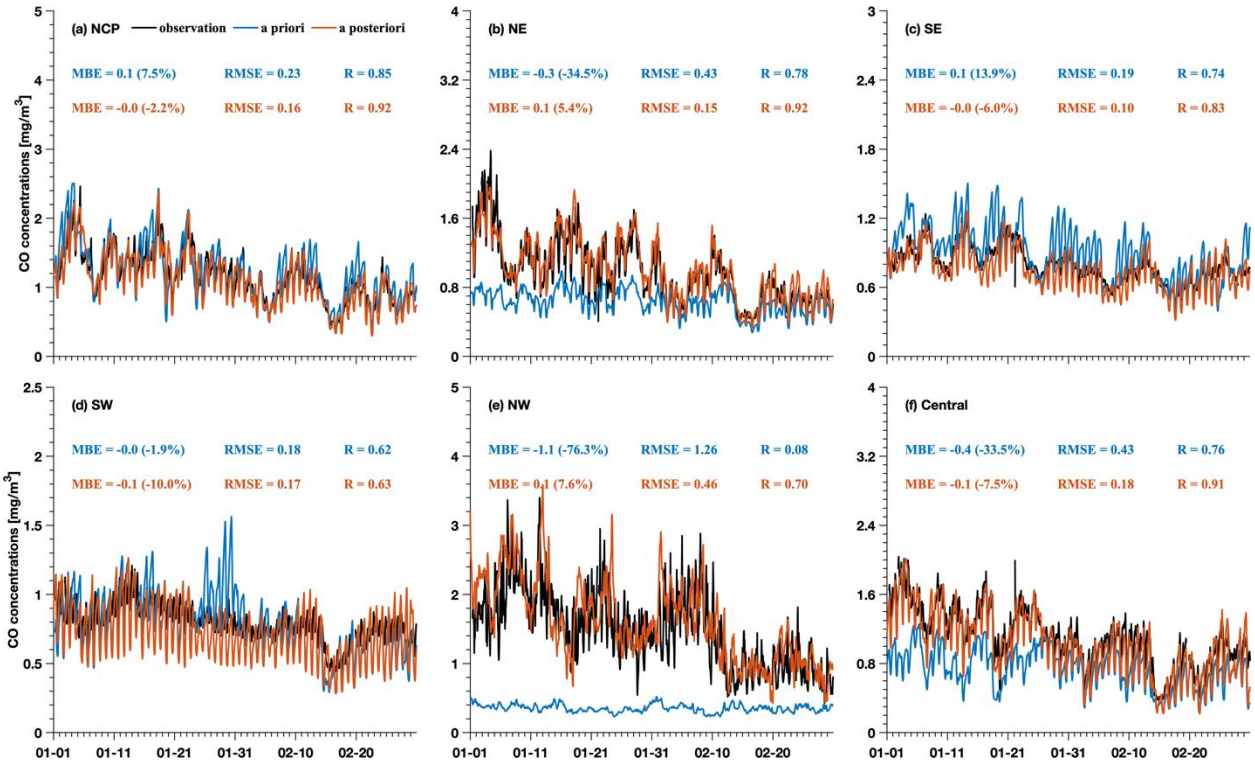

Figure S5: Same as in Fig. S1 but for CO concentrations.

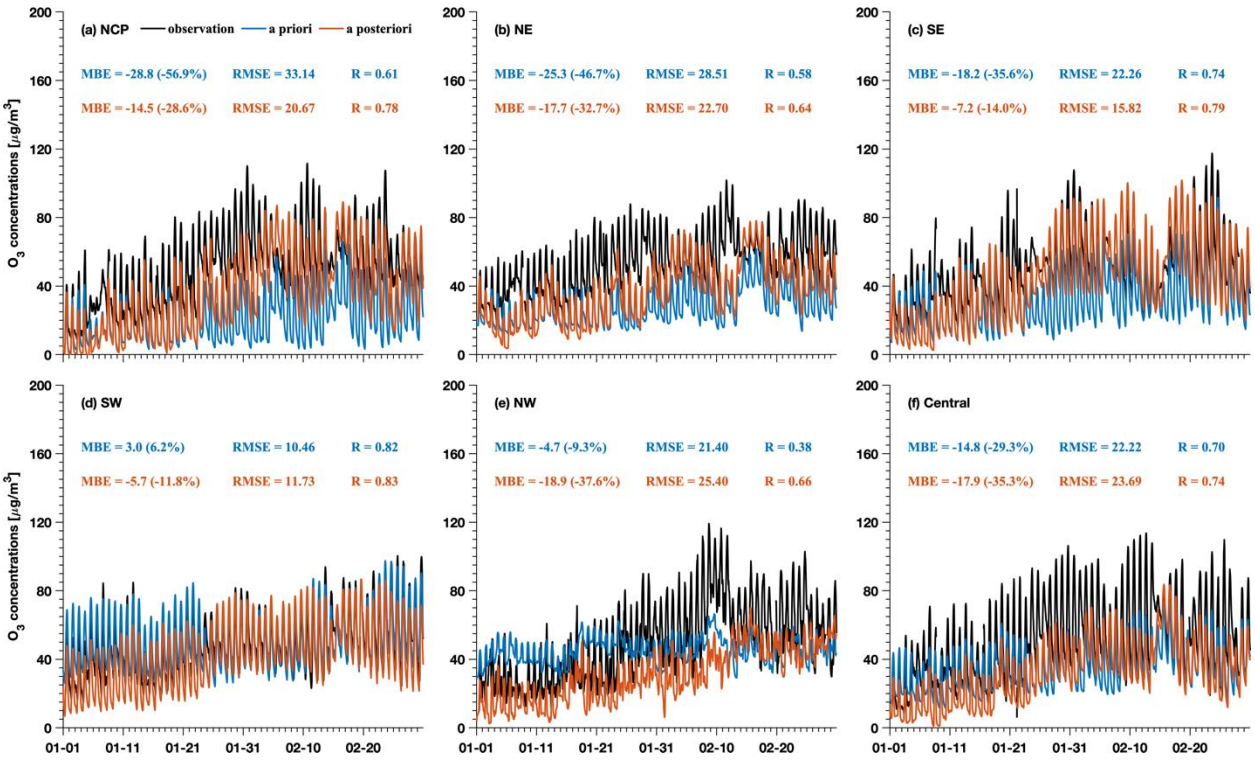

Figure S6: Same as in Fig. S1 but for O_3 concentrations.

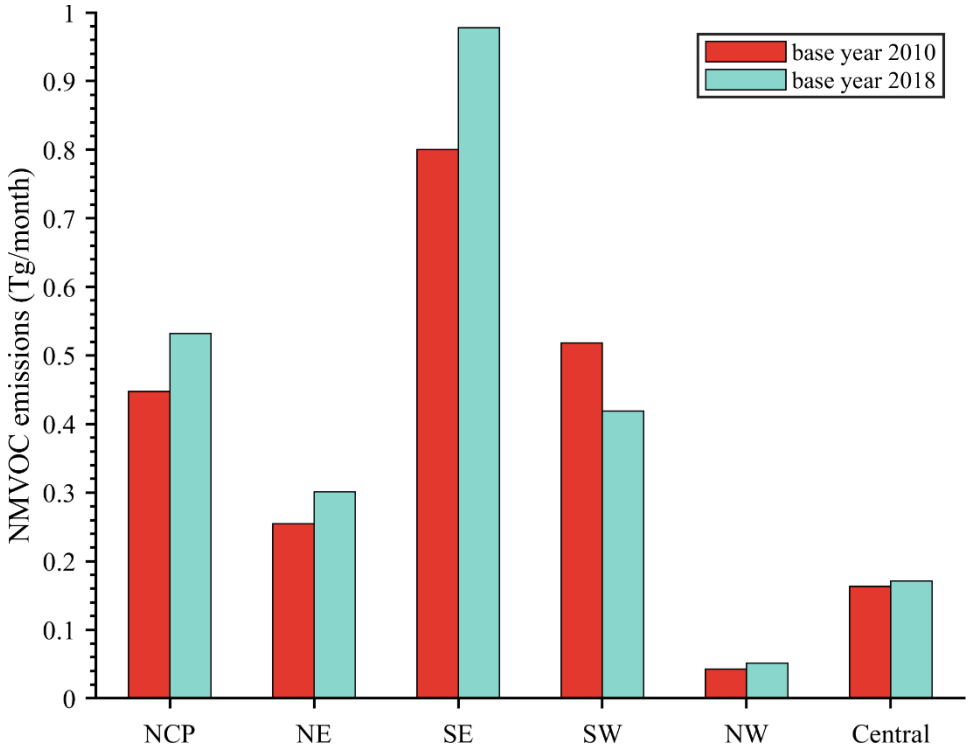

Figure S7: comparisons of the NMVOC emissions for base year 2010 with those for 2018 over different regions of China.

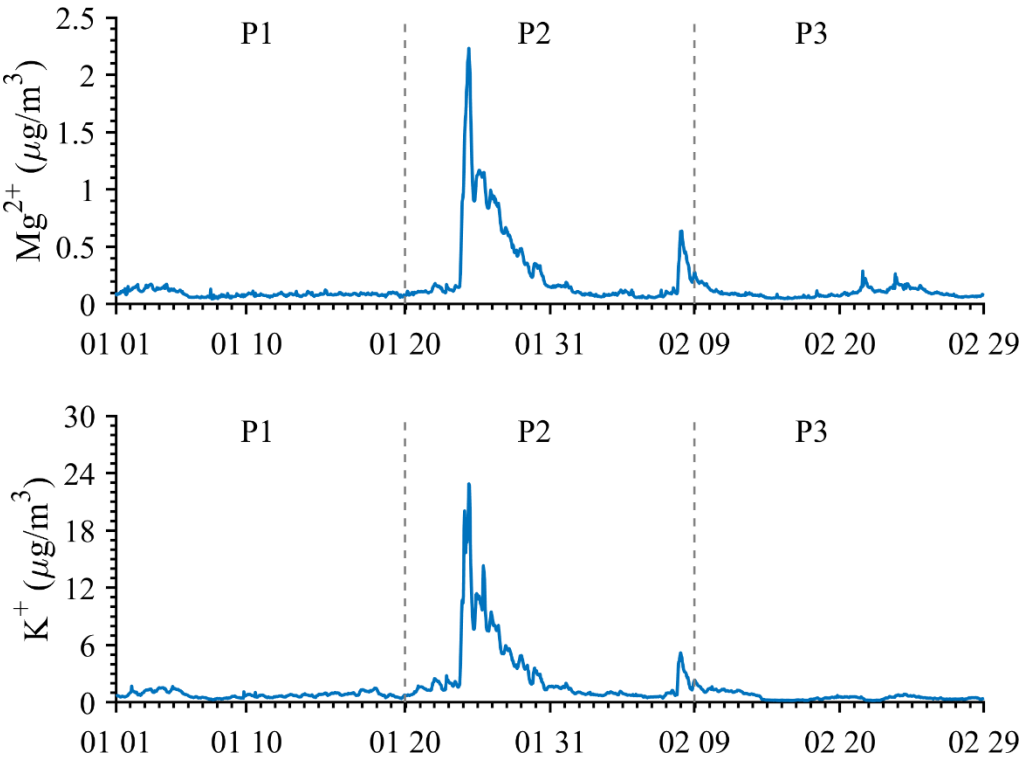

Figure S8: Timeseries of averaged concentrations of potassium and magnesium ion during COVID-19 pandemic over the NCP region. Measurements of potassium and magnesium ion were obtained from the CNEMC.

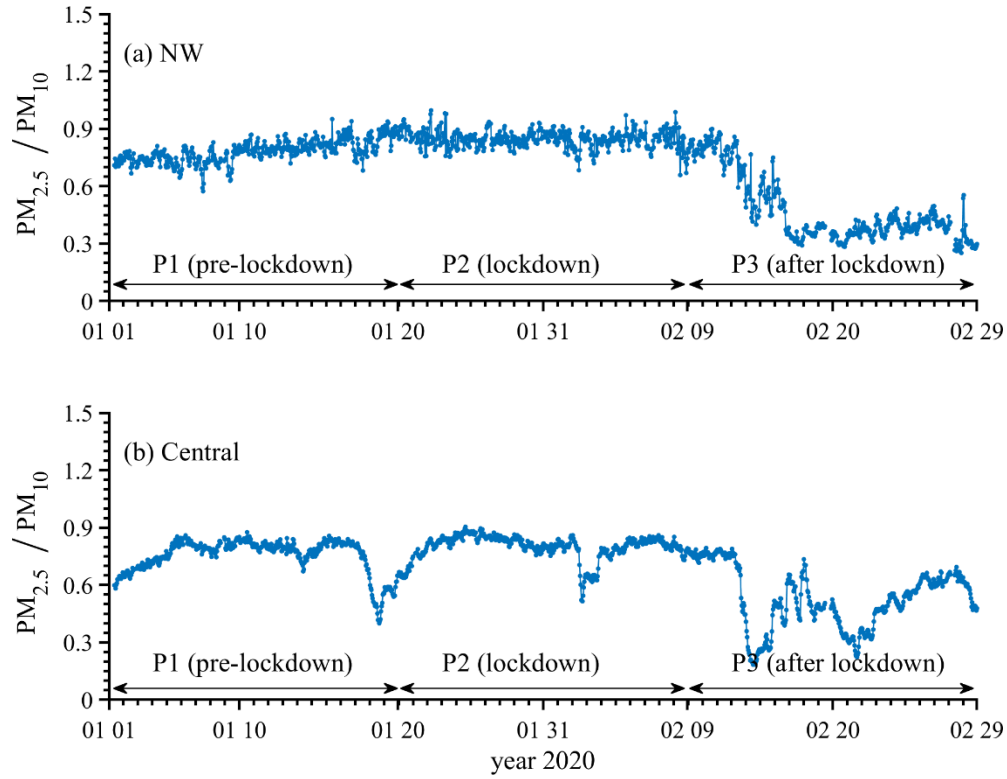

Figure S9: Timeseries of $PM_{2.5}/PM_{10}$ ratio during COVID-19 pandemic over (a) NW and (b) Central region.

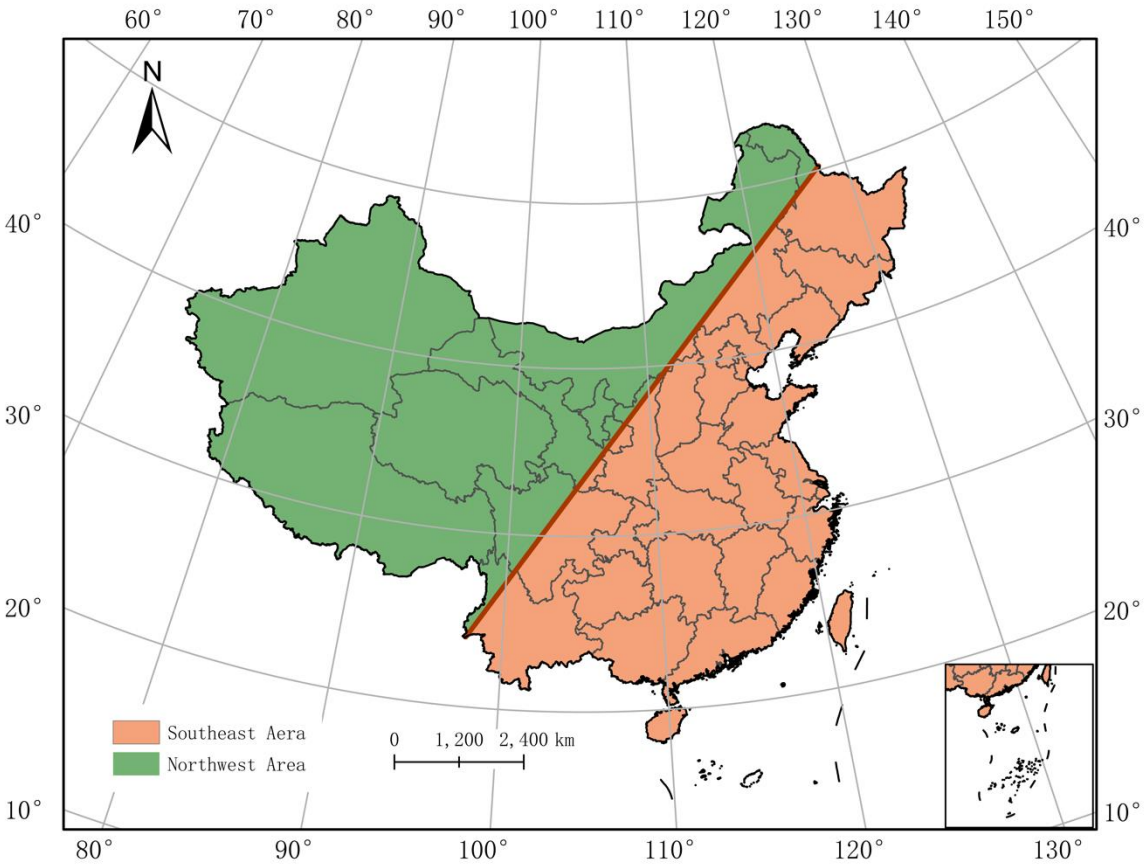

Figure S10: Geographical definition of southeast China (orange part) and northwest (green part) based on the Hu Huanyong Line. This line divides the China based on the population with population in east of this line (southeast China) accounts for 86.72% of the total population in China.

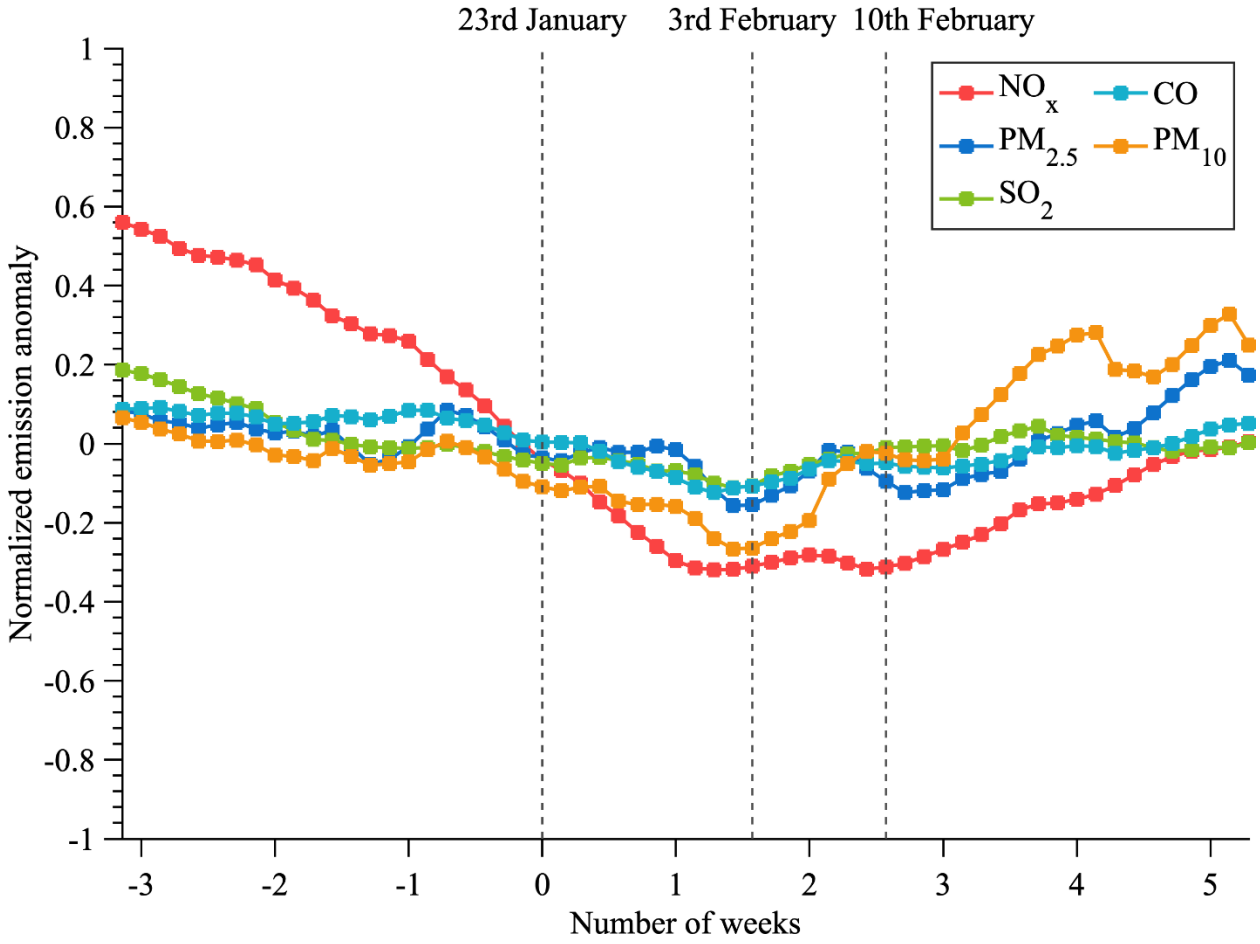

Figure S11: Time series of normalized emission anomaly estimated by inversion results for different species in southeast China (defined in Figure S10) from 1st January to 29th February 2020. The normalized emission anomaly is calculated by the emission anomaly divided by the averaged emission during the whole period.

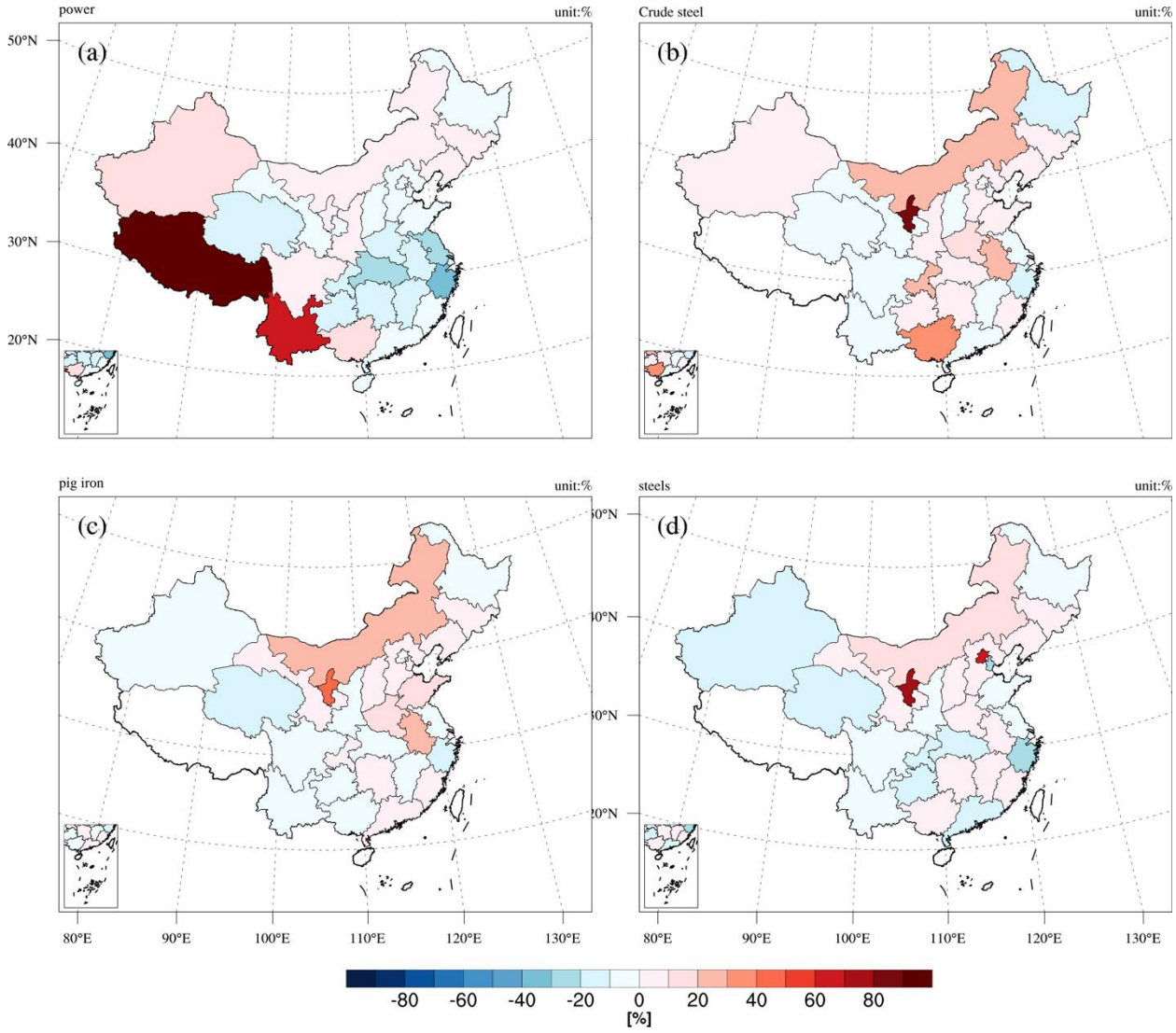

78

79 **Figure S12: Changes in (a) thermal power generation, productions of (b) crude steel, (c) pig iron, and (d) steels in China in the first two months**
80 **of 2020 compared to those in 2019.**

81

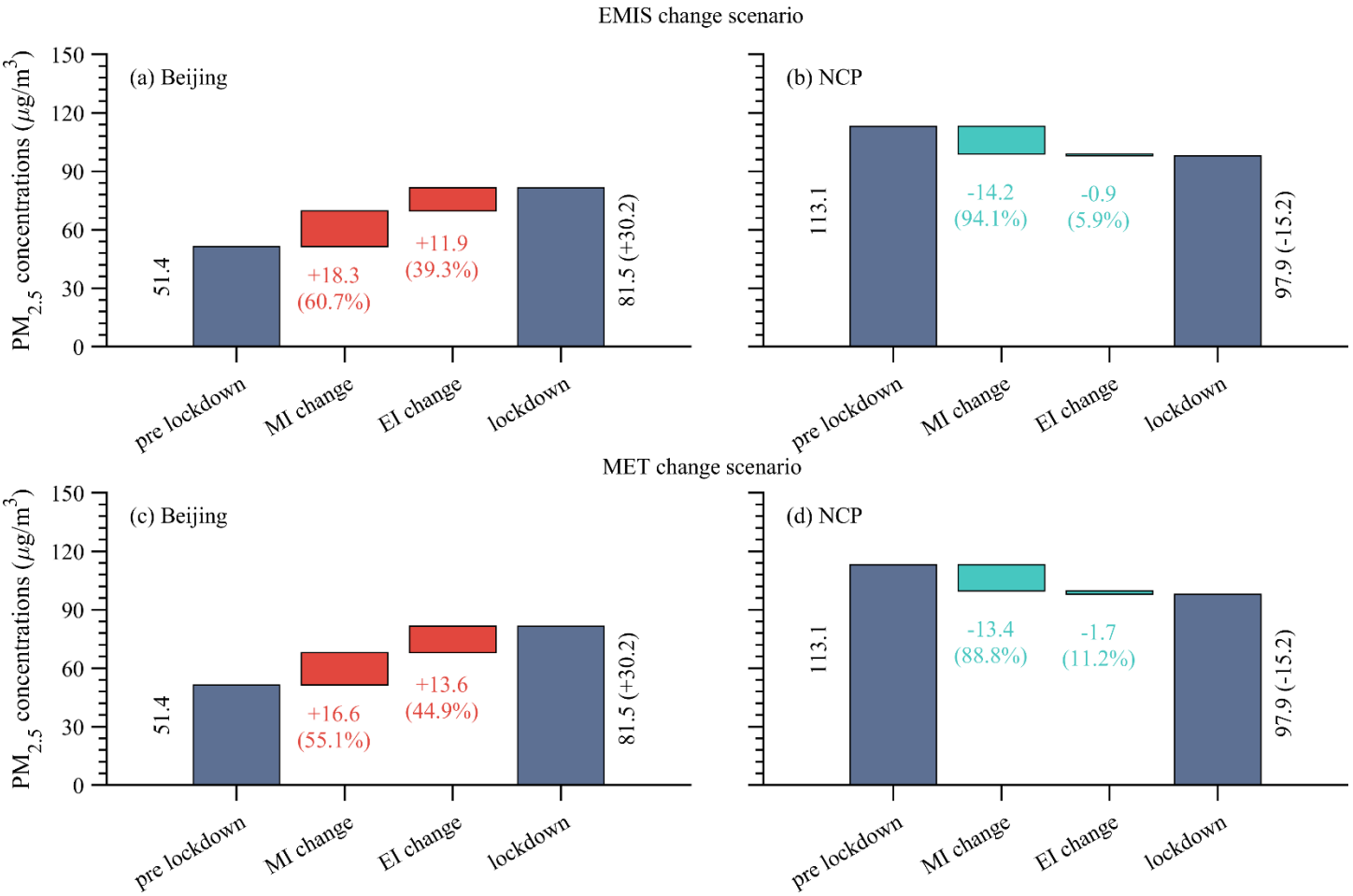

Figure S13: The calculated MI and EI changes of $PM_{2.5}$ concentrations over the (a, c) Beijing and (b, d) the NCP region using the EMIS change scenario (upper panel) and MET change scenario (lower panel).

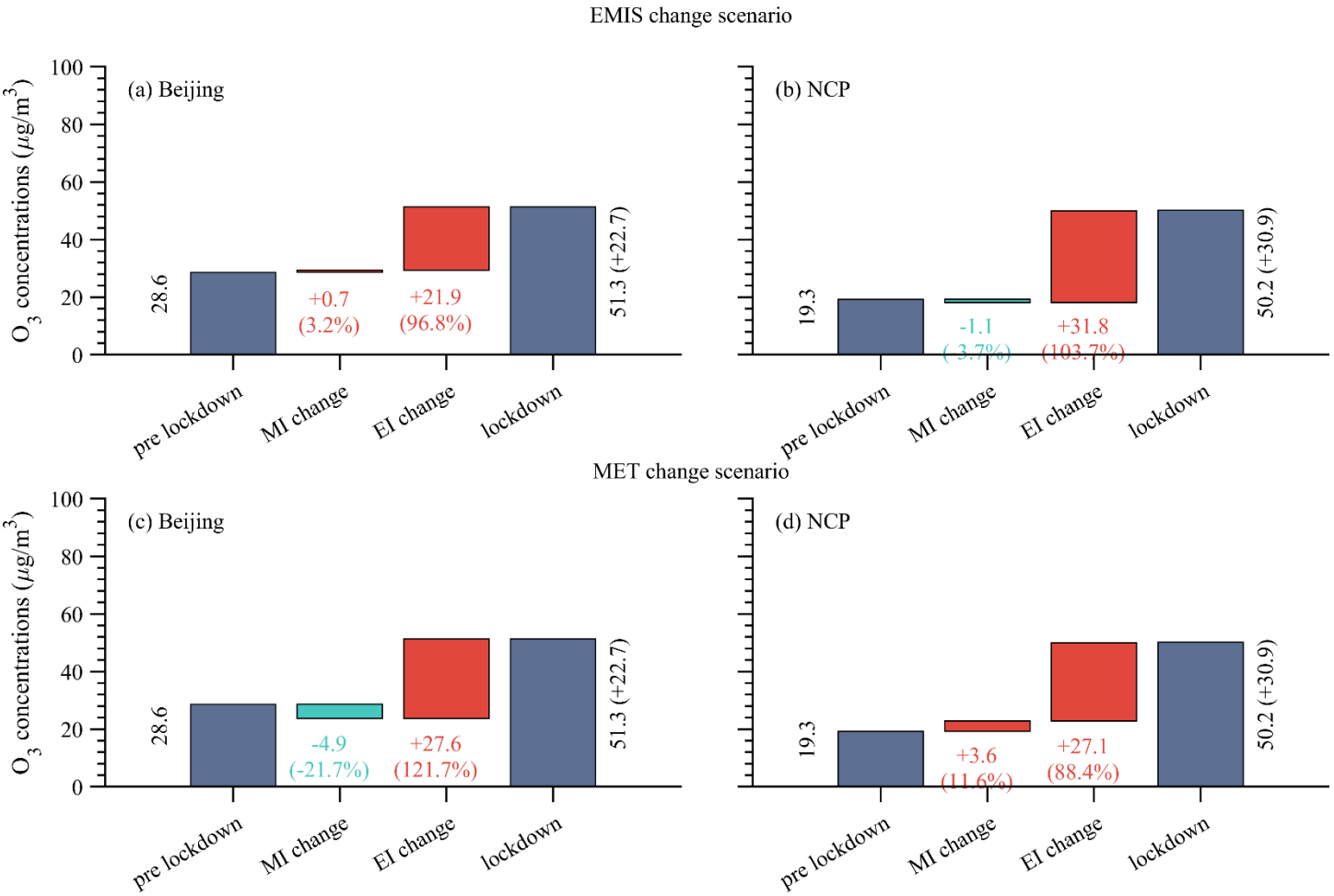

Figure S14: The calculated MI and EI changes of O_3 concentrations over the (a, c) Beijing and (b, d) the NCP region using the EMIS change scenario (upper panel) and MET change scenario (lower panel).

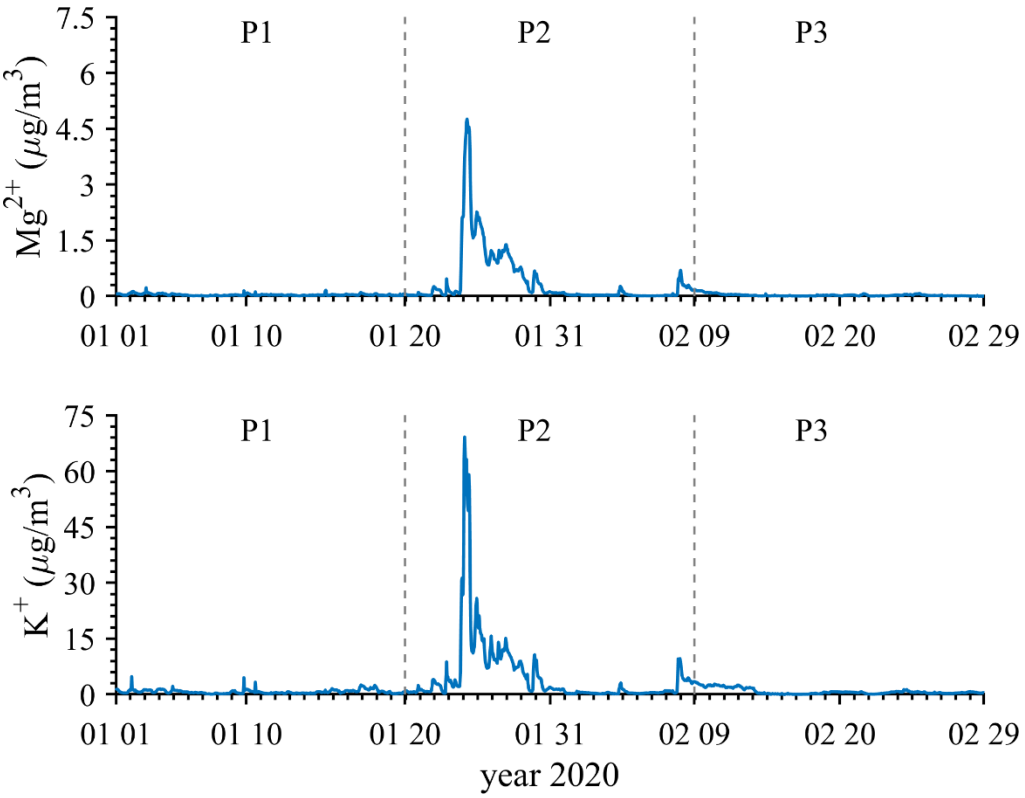

Figure S15: Timeseries of averaged concentrations of potassium and magnesium ion during COVID-19 pandemic over the Beijing. Measurements of potassium and magnesium ion were obtained from CNEMC.

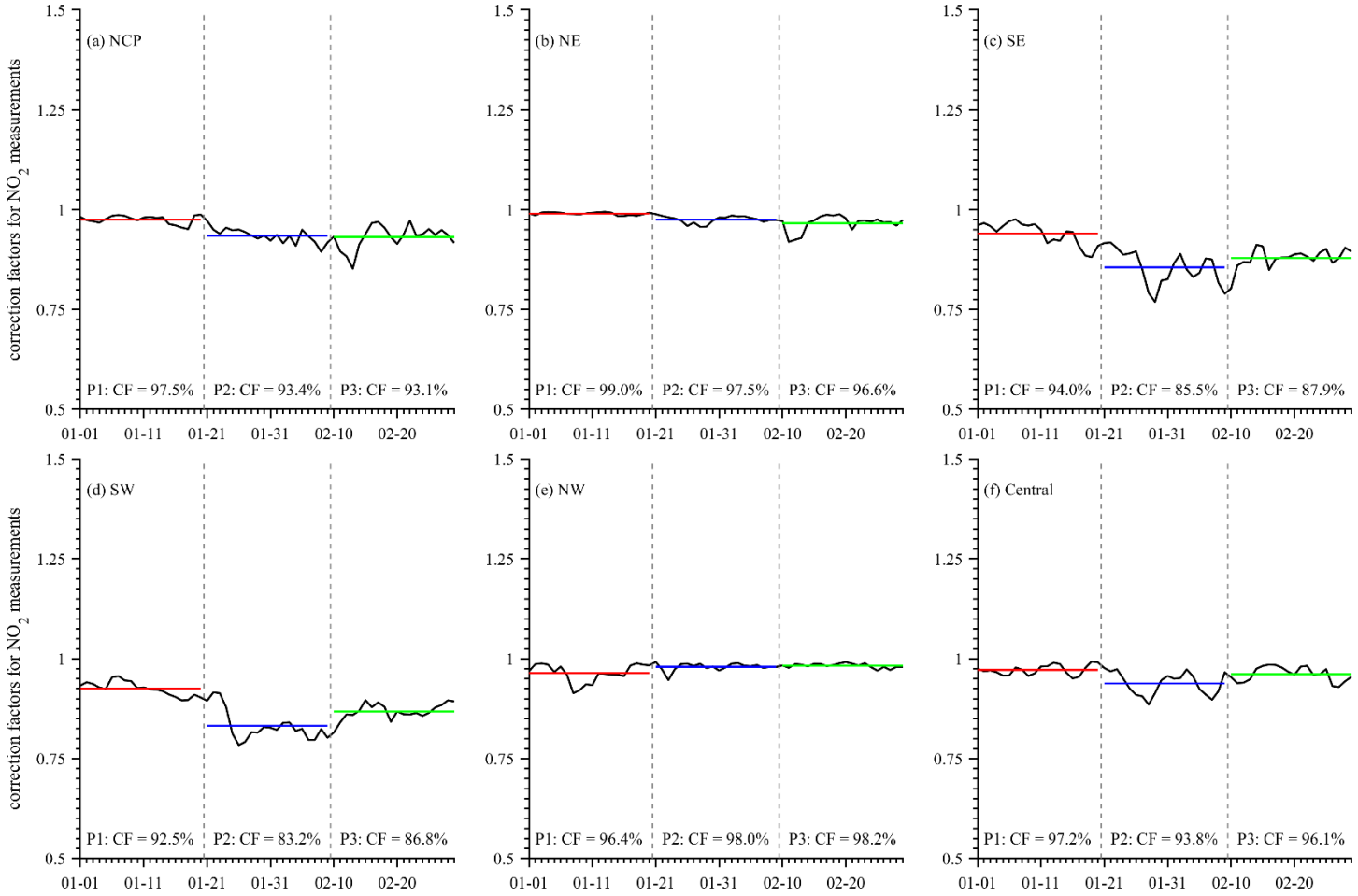

Figure S16: Time series of calculated CFs for NO_2 measurements over (a) NCP, (b) NE, (c) SE, (d) SW, (e) NW and (f) Central region during COVID-19 pandemic. The averaged CF values during different stages of COVID-19 pandemic are also labelled.

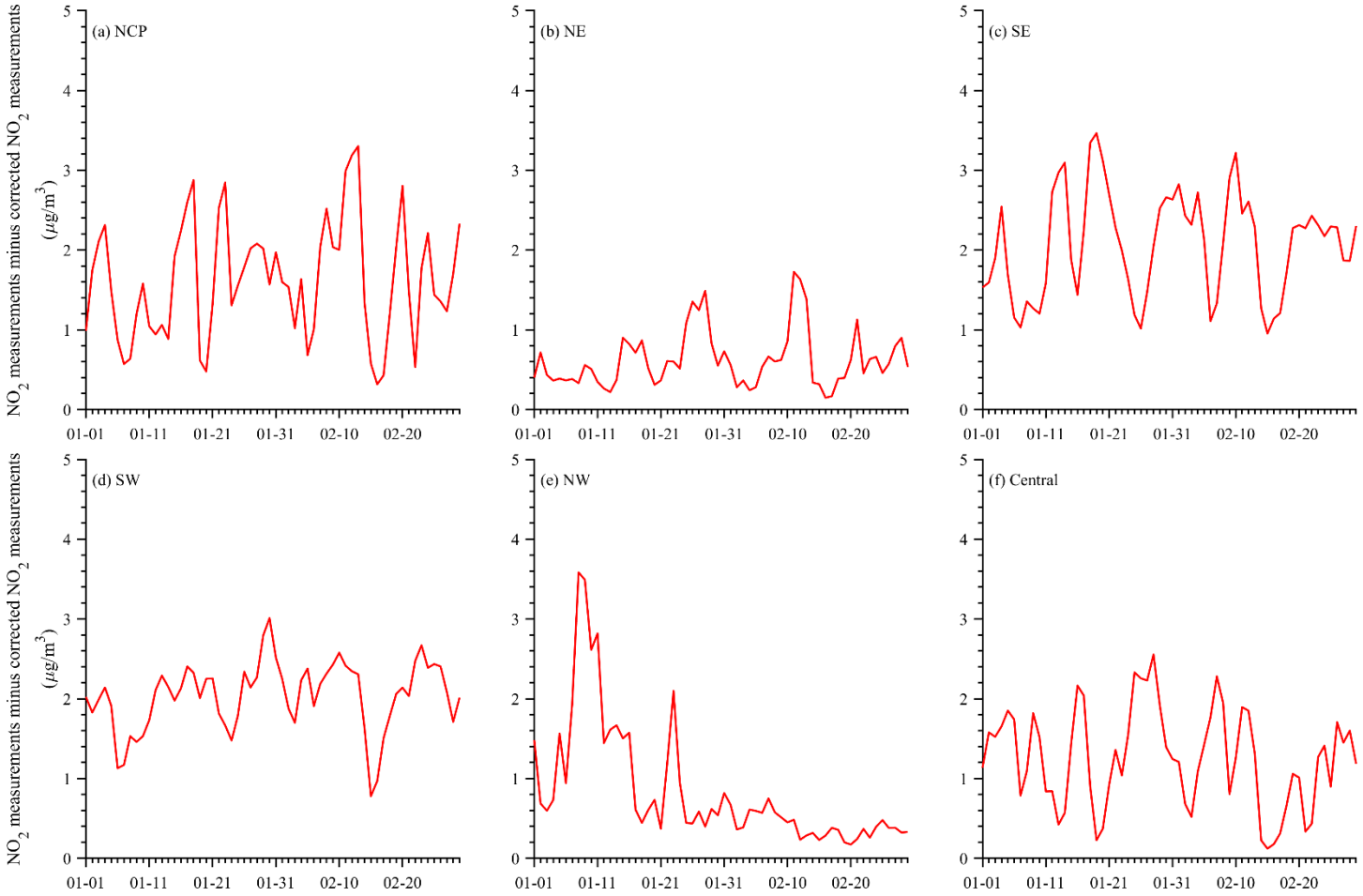

Figure S17: the difference of NO_2 measurement before and after the corrections of chemiluminescence monitor interference over (a) NCP, (b) NE, (c) SE, (d) SW, (e) NW and (f) Central during the COVID-19 period.

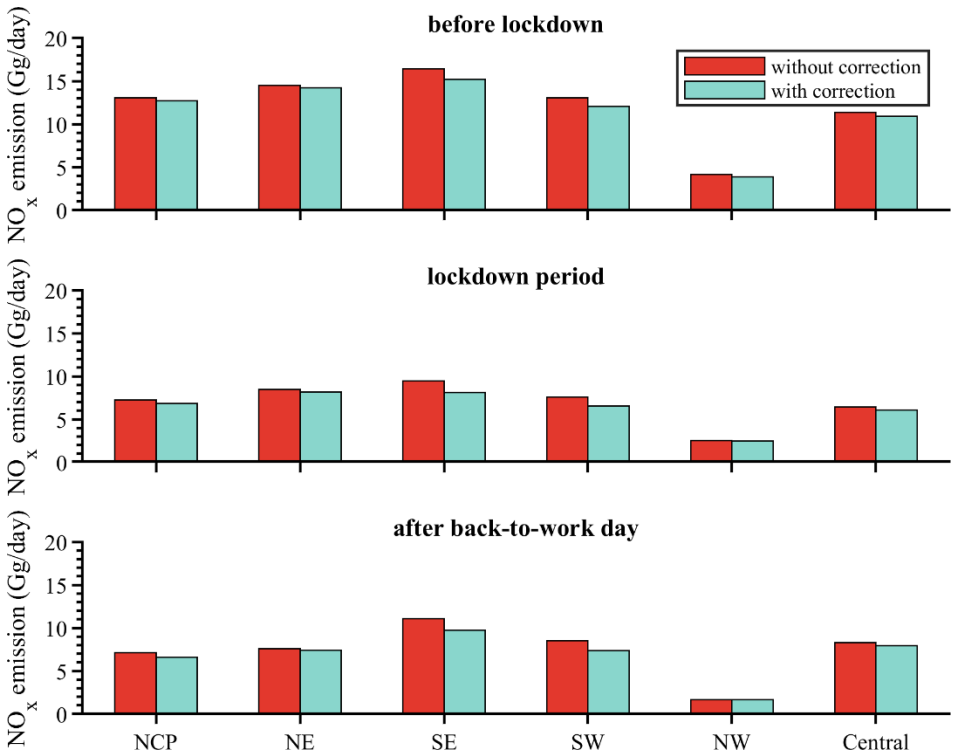

Figure S18: Comparisons of inversed NO_x emissions with (blue) and without (red) correction of NO_2 measurement over different regions of China during different period of COVID-19 pandemic.

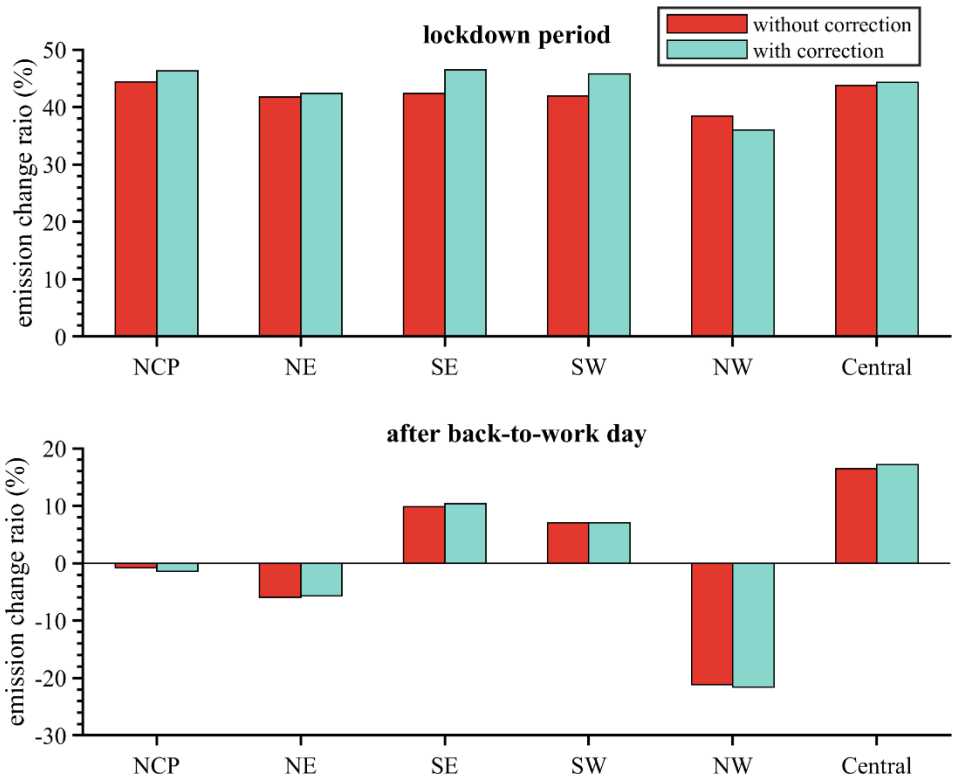

Figure S19: Comparisons of the calculated emission change of NO_x emissions based on the inversion results with (blue) and without (red) correction of NO_2 measurement over different regions of China.

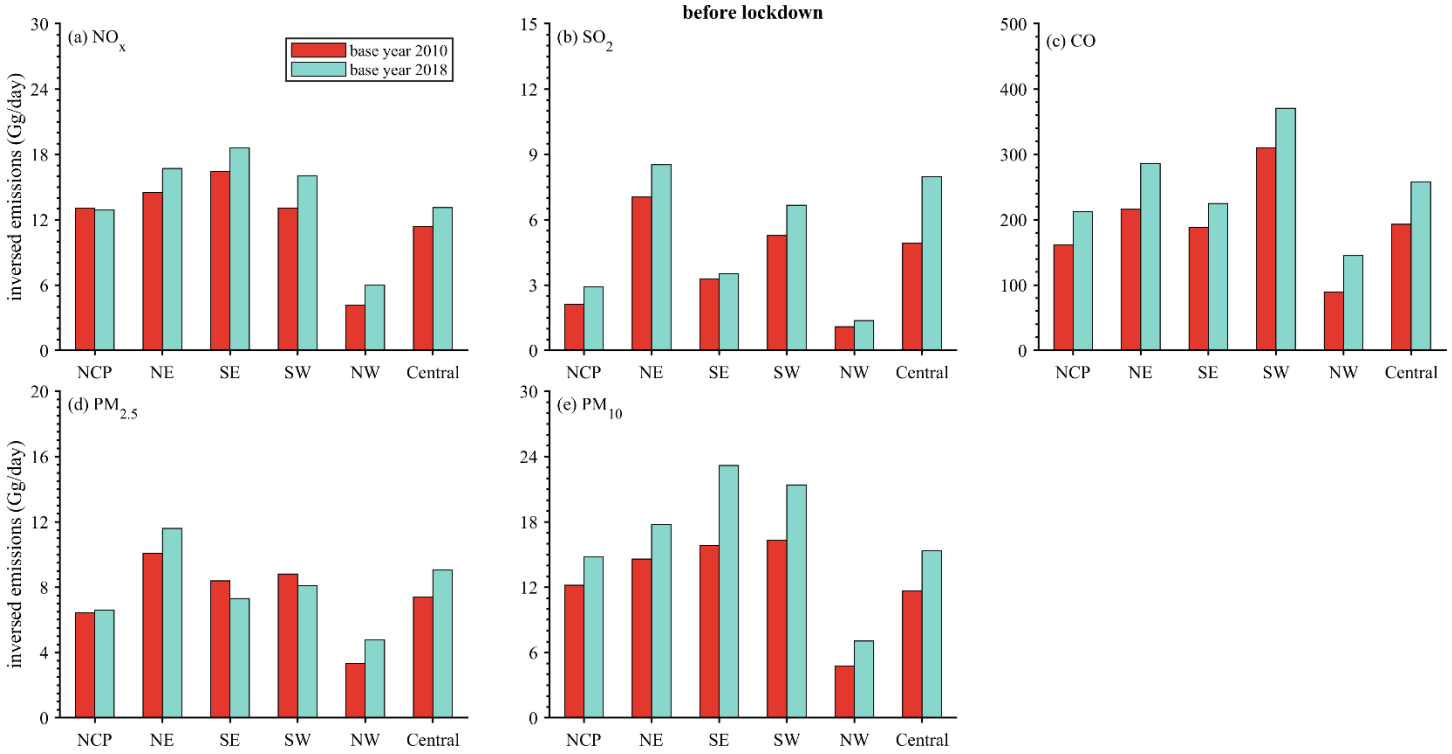

Figure S20: Comparisons of the inversion estimated total emissions of (a) NO_x, (b) SO_2, (c) CO, (d) $PM_{2.5}$ and (e) PM_{10} before lockdown based on the a priori emissions for 2010 (read) with those based on the a priori emissions for 2018 (blue).

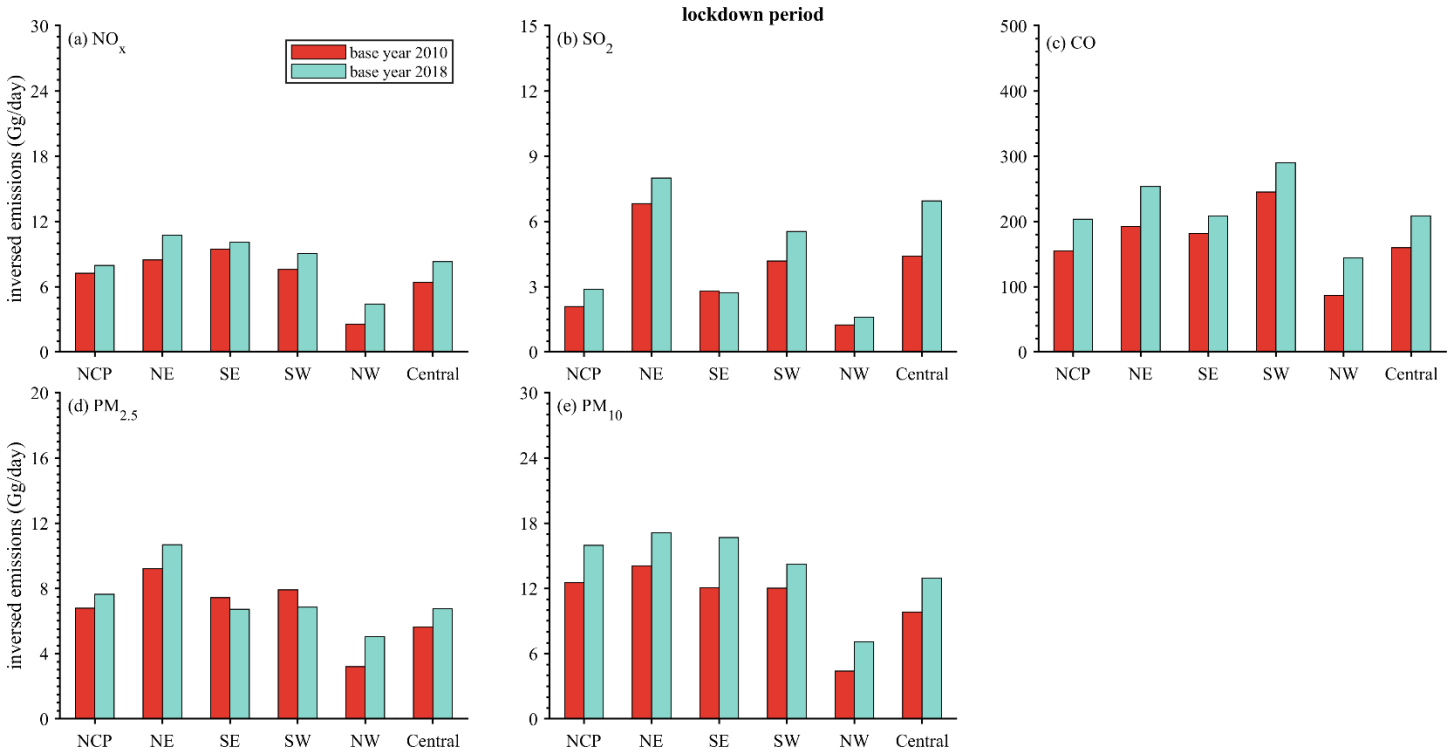

Figure S21: Same as Fig.S18 but for the lockdown period.

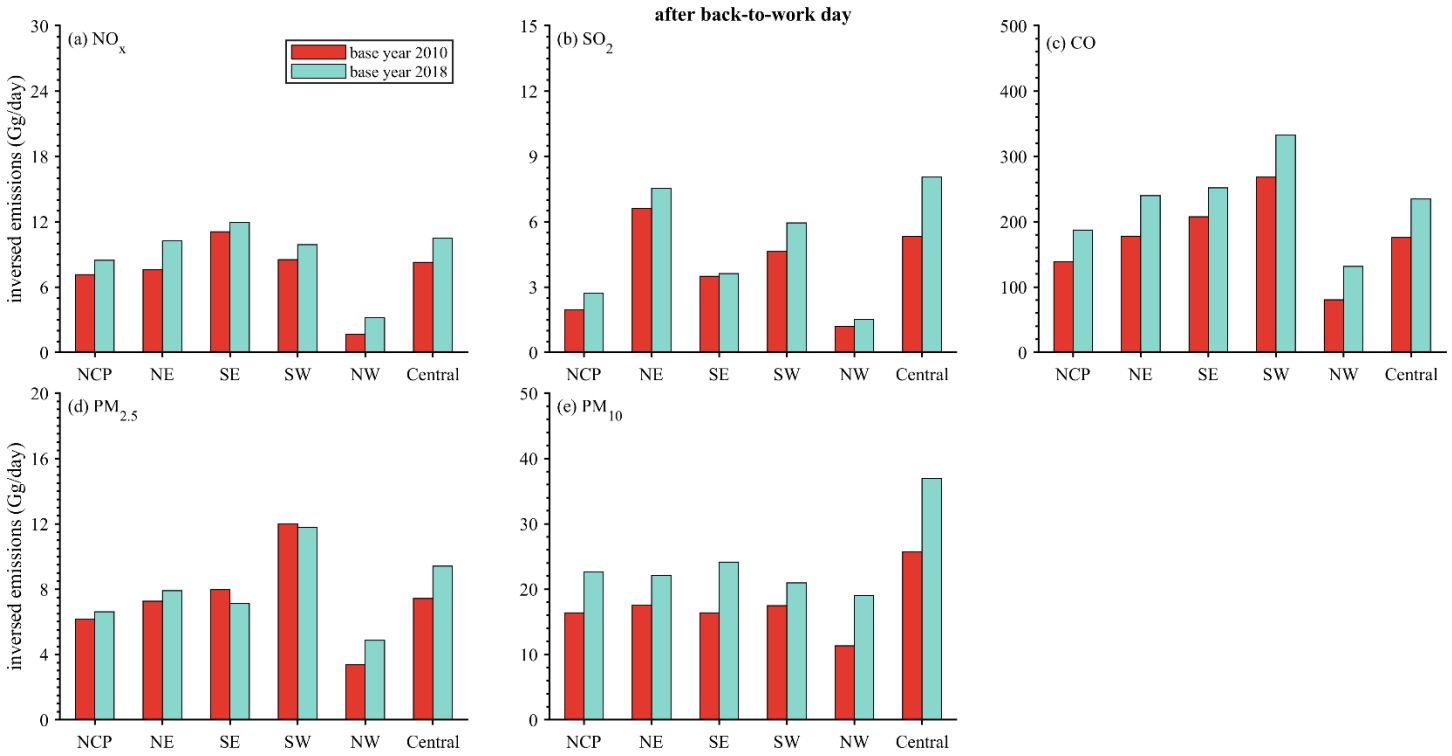

Figure S22: Same as Fig.S18 but for after back-to-work day.

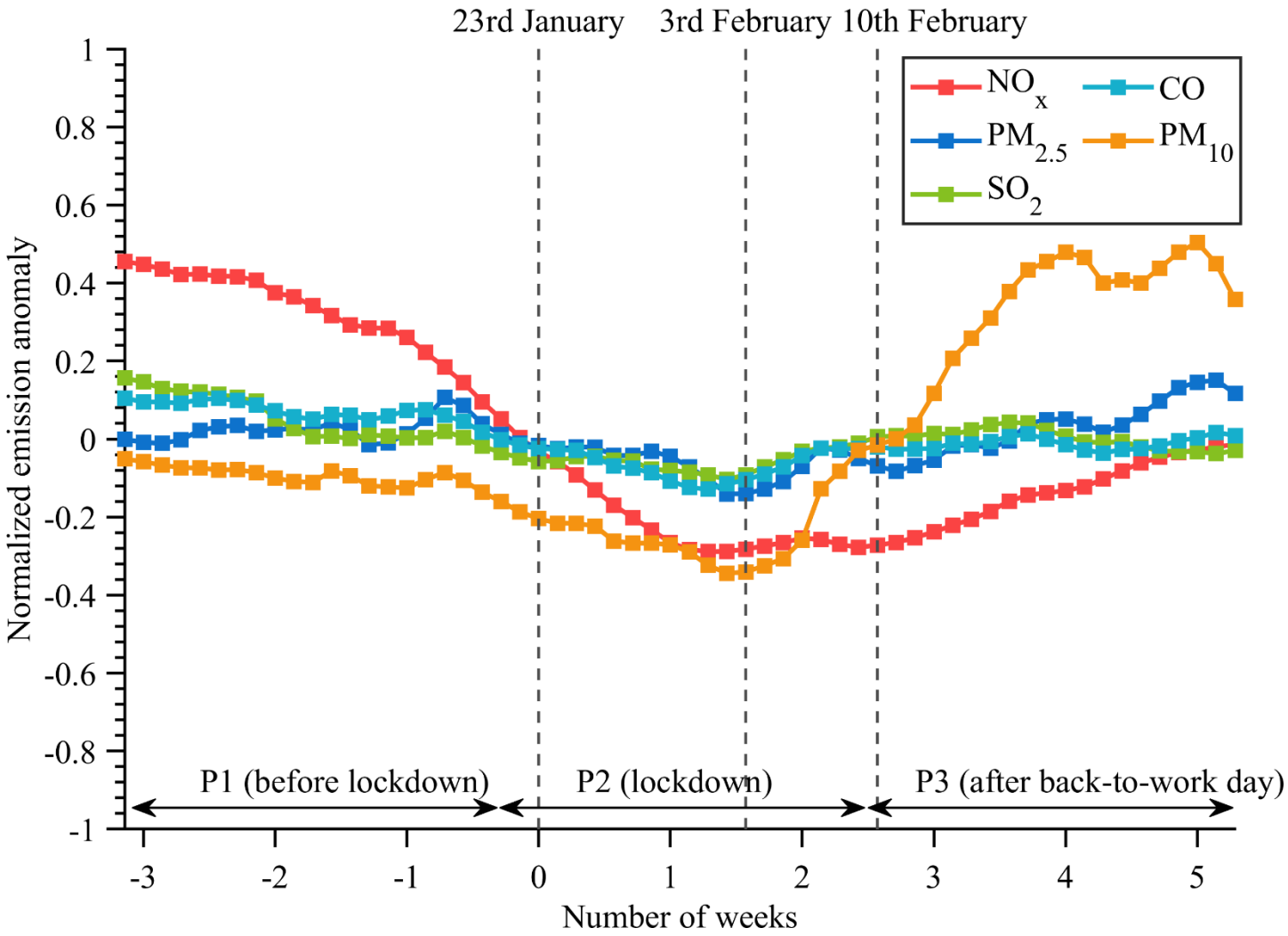

Figure S23: Time series of normalized emission anomalies estimated by inversion results for different species in China from 1st January to 29th February 2020 using the a priori emissions for 2018.

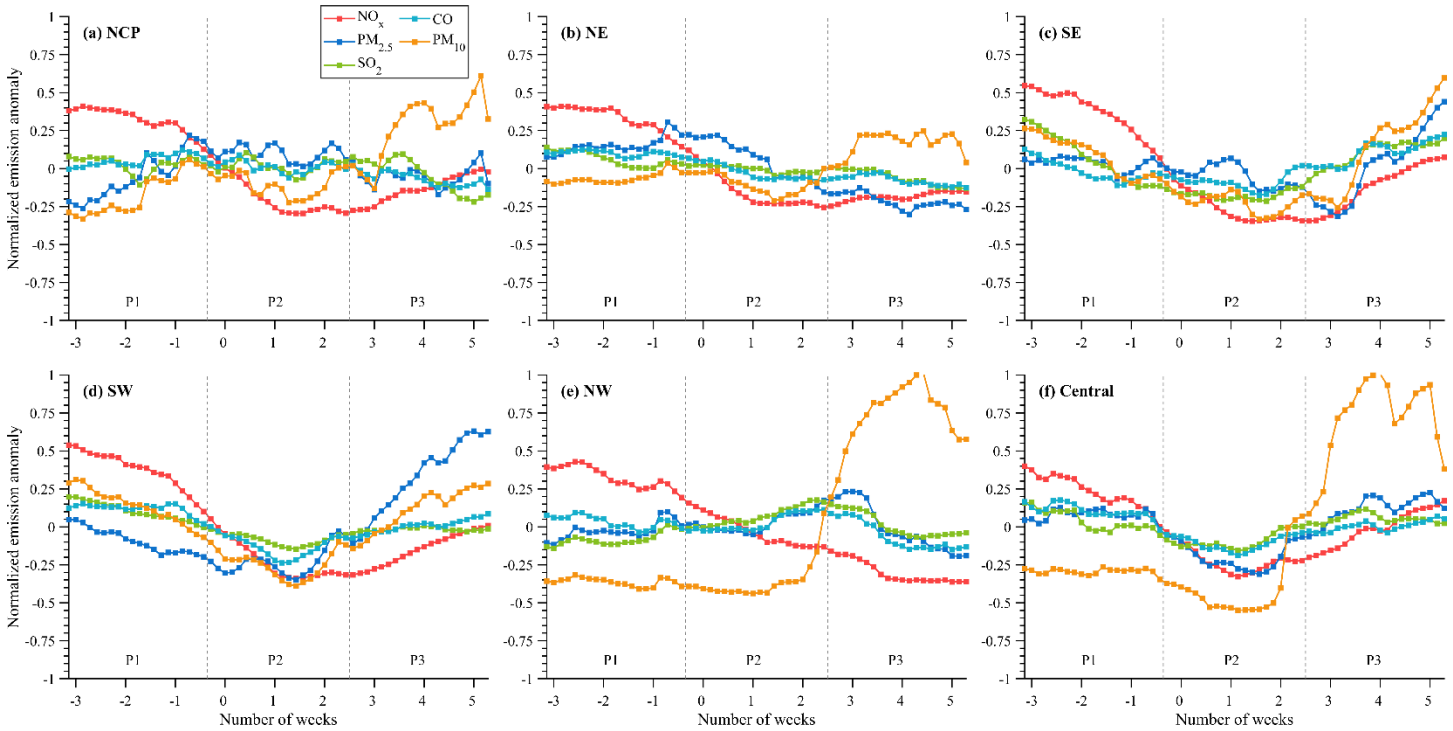

Figure S24: Time series of normalized emission anomalies estimated by inversion results for different species over (a) NCP region, (b) NE region, (c) SE region, (d) SW region, (e) NW region and (f) Central region from 1st January to 29th February 2020 using the a priori emissions for 2018.

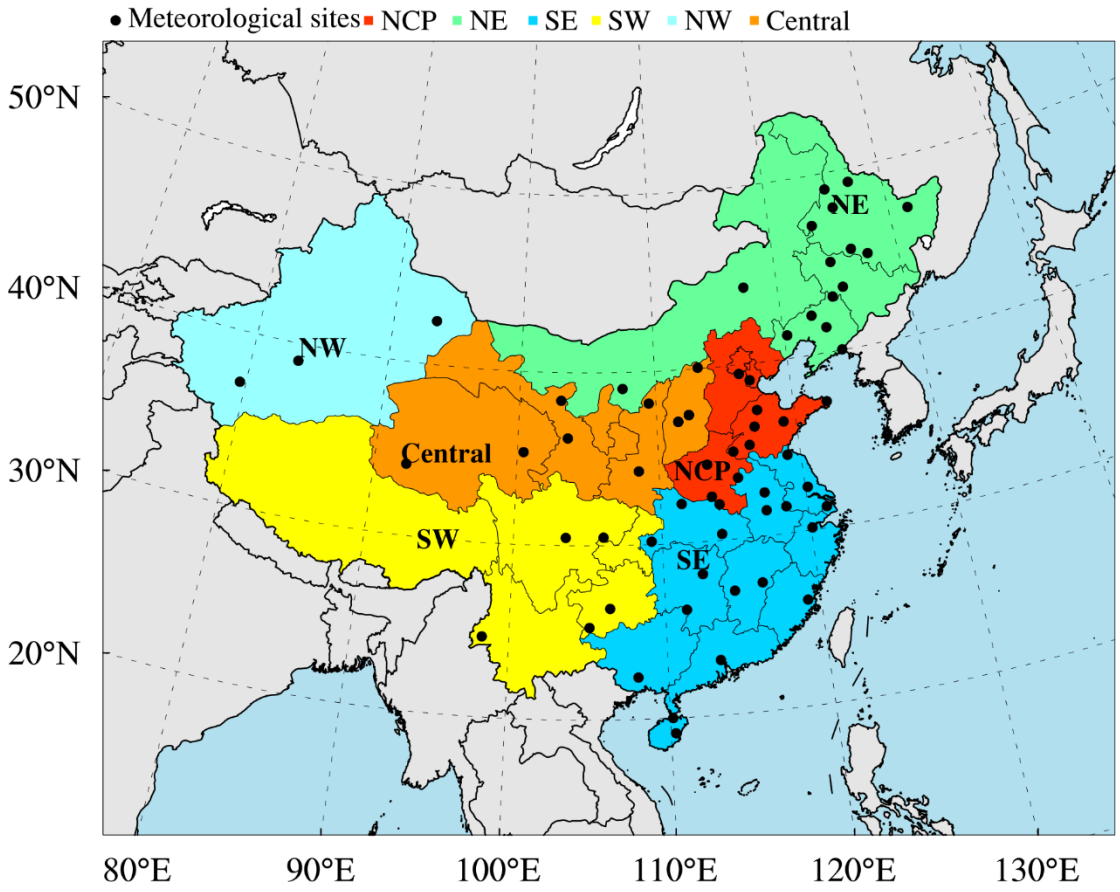

126

127 **Figure S25: Spatial distribution of meteorological observation sites used in the evaluation of meteorology simulations over different regions of**
128 **mainland China.**

129

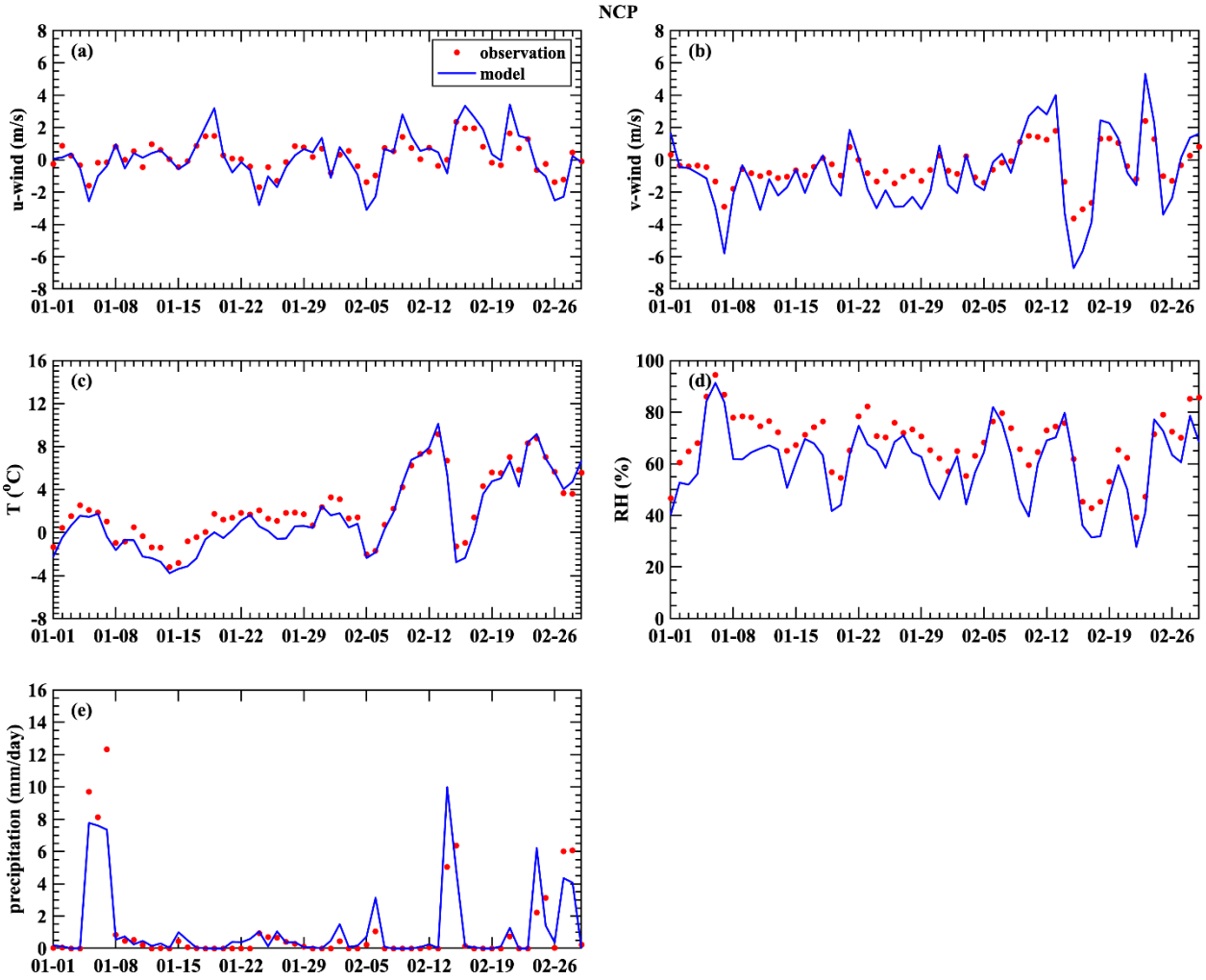

Figure S26: Timeseries of observed (red dots) and simulated (blue line) values of (a) u-wind, (b) v-wind, (c) temperature, (d) relative humidity and (e) precipitation over NCP region from 1st Jan 2020 to 29th Feb 2020.

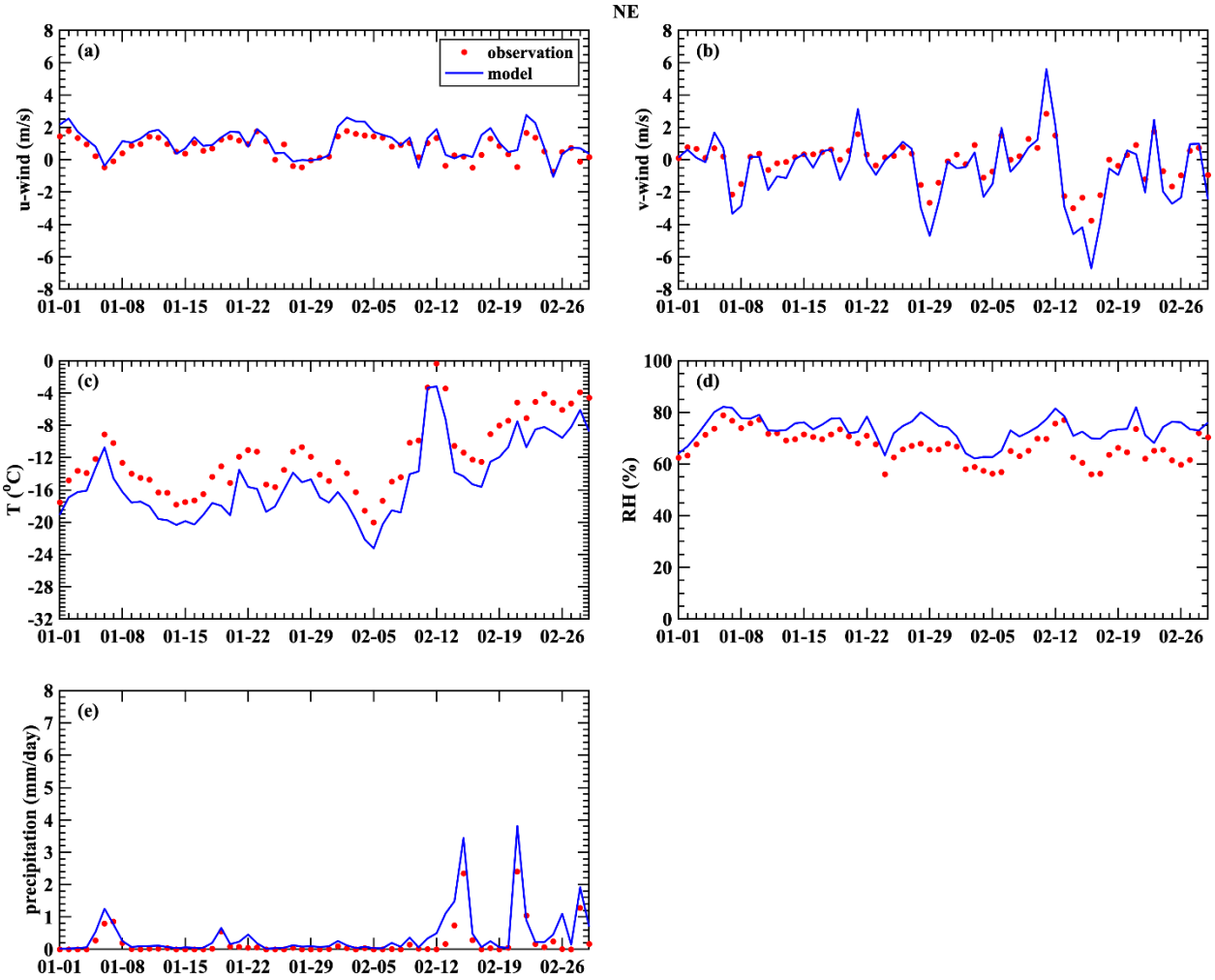

Figure S27: Same as in Figure S20 but over the NE region.

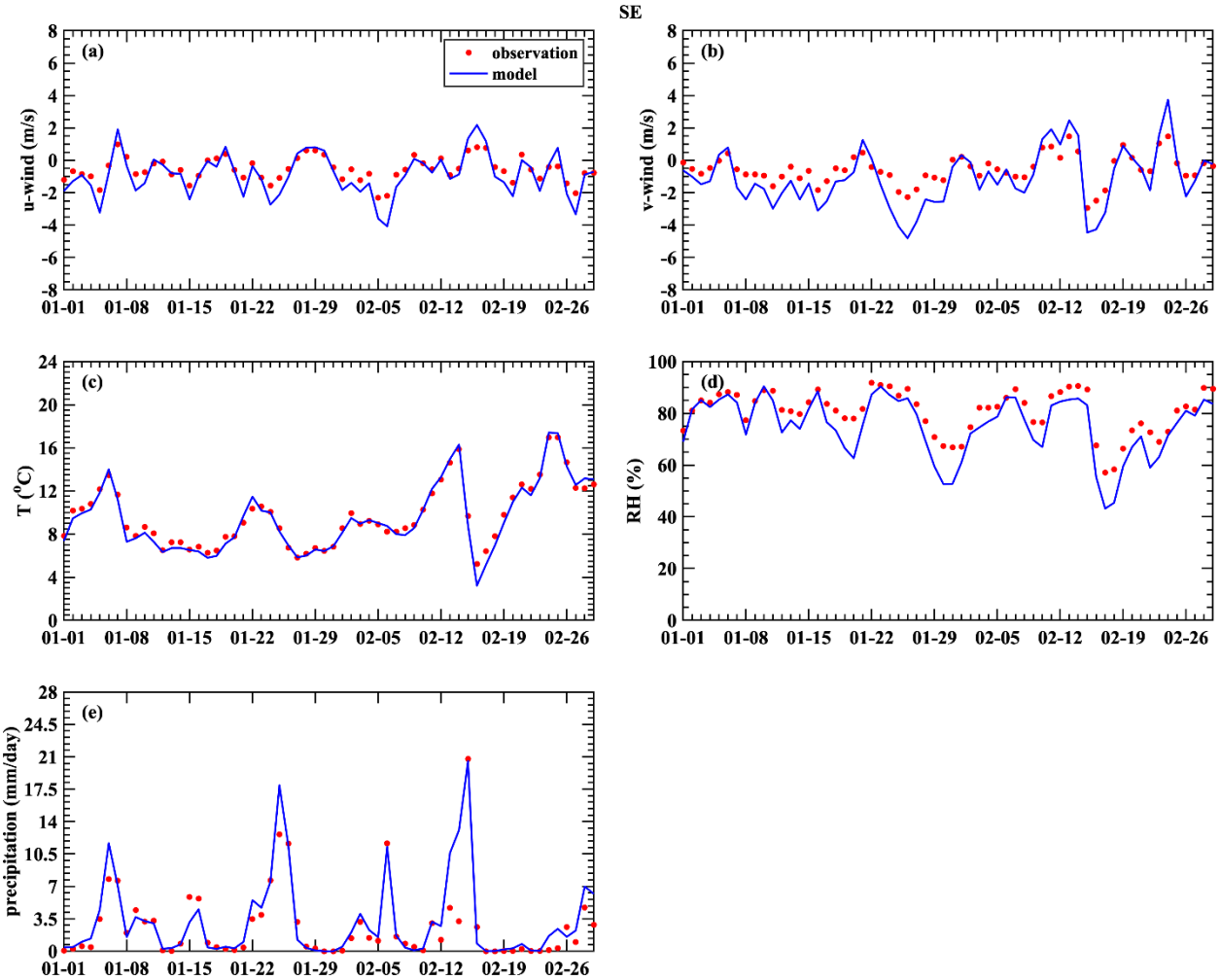

Figure S28: Same as in Figure S20 but over the SE region.

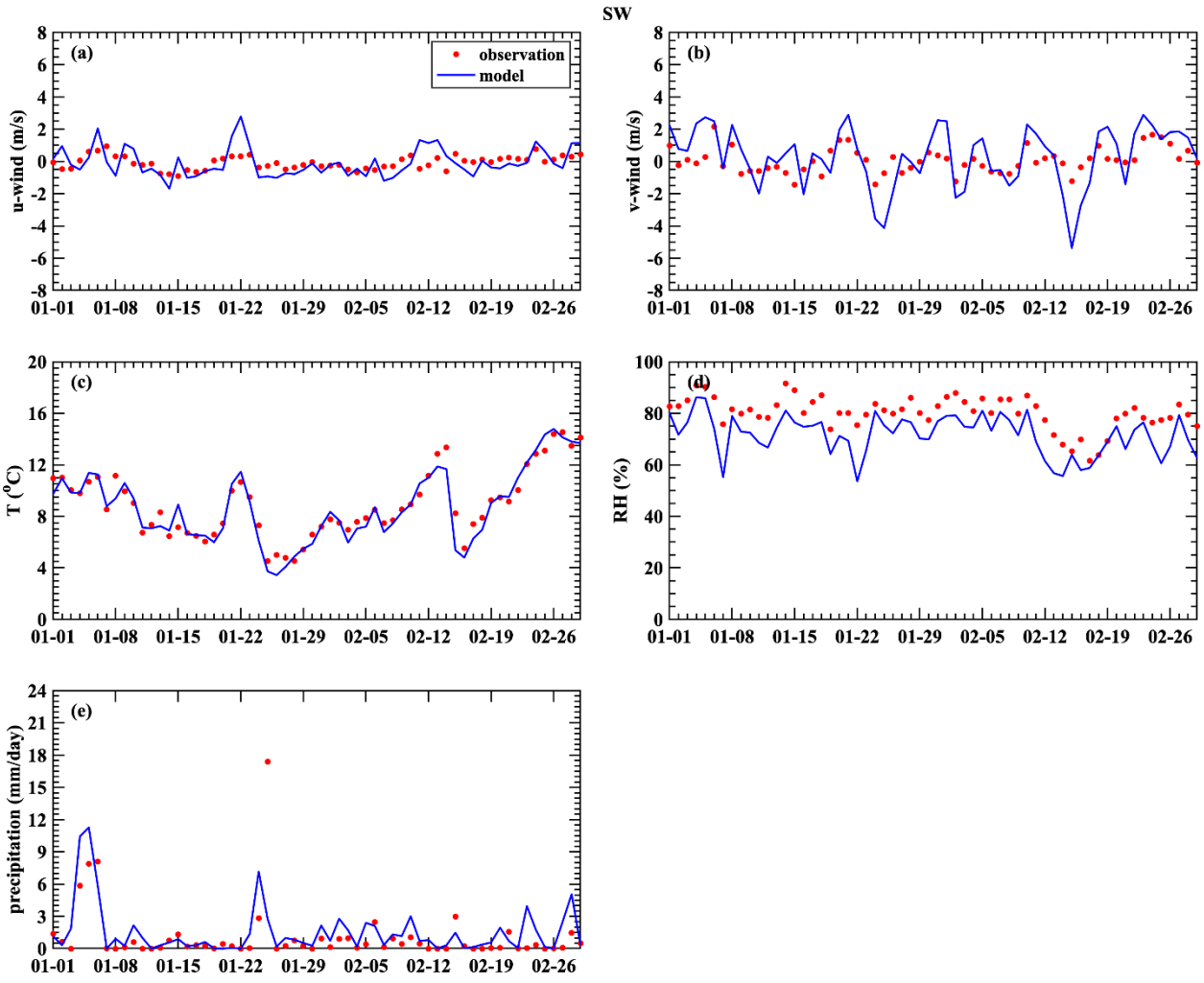

Figure S29: Same as in Figure S20 but over the SW region.

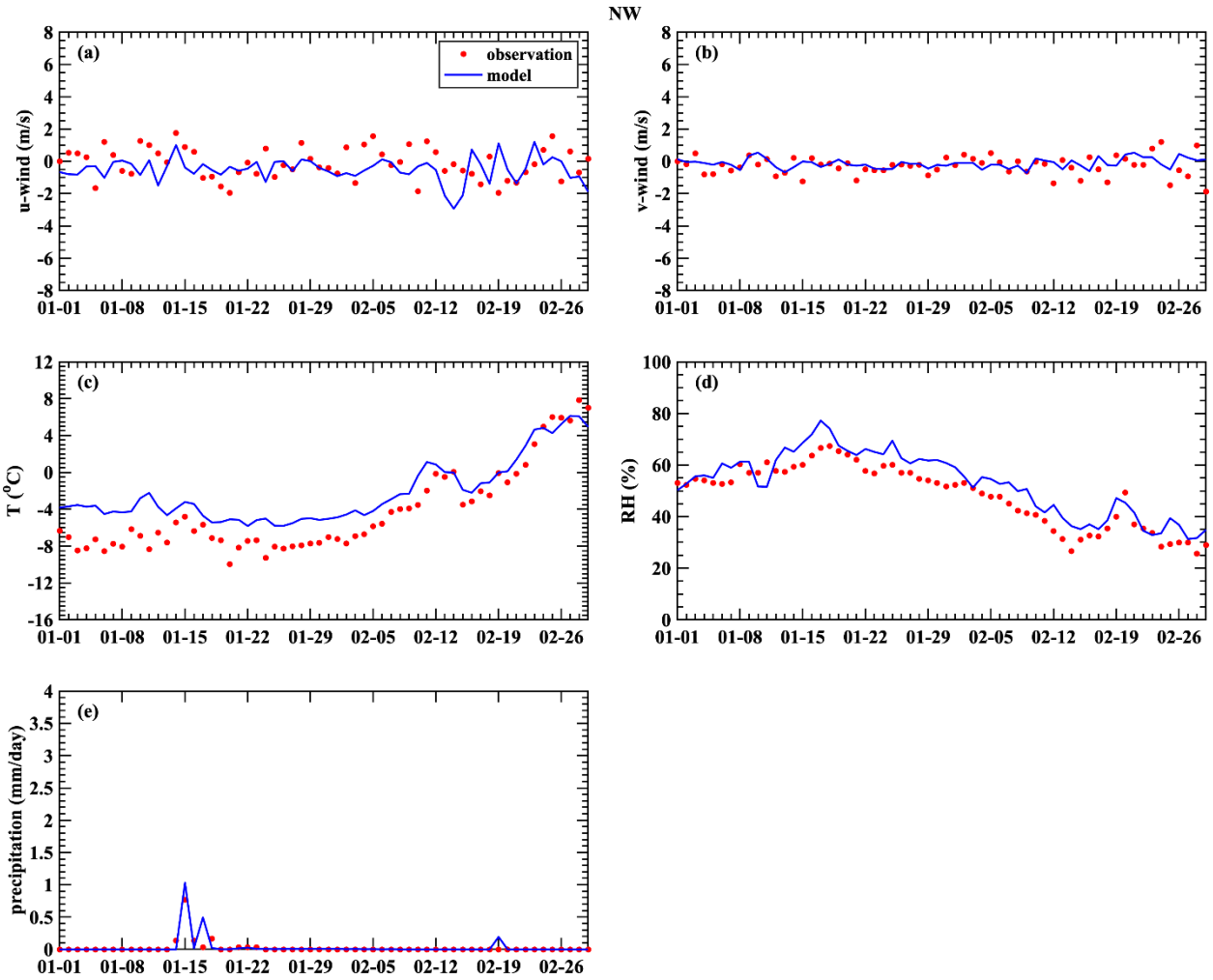

Figure S30: Same as in Figure S20 but over the NW region.

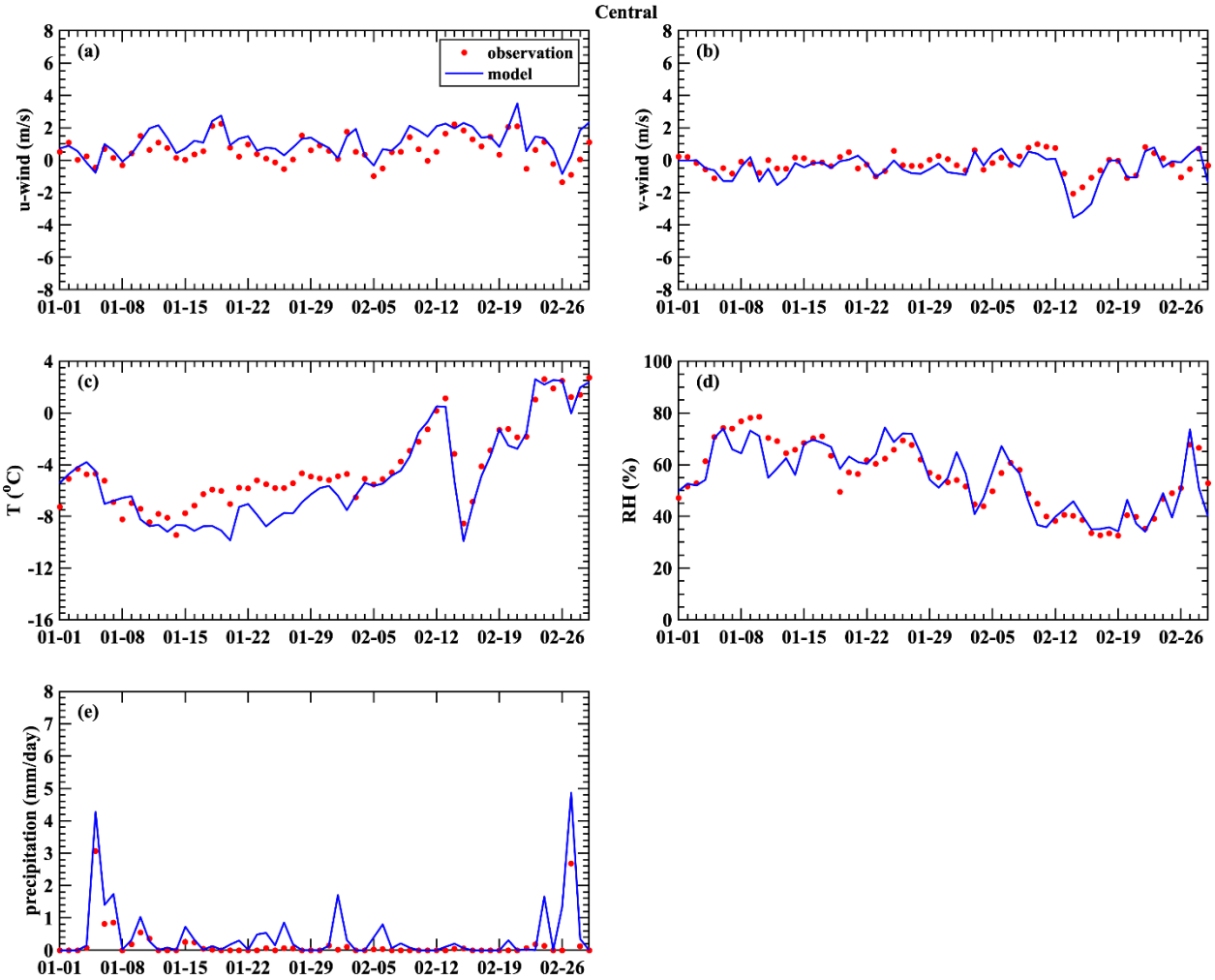

Figure S31: Same as in Figure S20 but over the Central region.

Tables

Table S1: Evaluation statistics of cross-validation run (outside of bracket) and a priori simulation (inside bracket)

	$PM_{2.5}$ ($\mu g/m^3$)				PM_{10} ($\mu g/m^3$)			
	R	MBE	NMB(%)	RMSE	R	MBE	NMB (%)	RMSE
NCP	0.94 (0.81)	5.3 (66.5)	7.1 (90.0)	14.4 (77.4)	0.92 (0.77)	2.6 (65.1)	2.6 (66.6)	19.2 (79.8)
NE	0.91 (0.74)	4.1 (1.2)	7.1 (2.0)	13.2 (19.5)	0.87 (0.72)	4.3 (-6.9)	5.7 (-9.0)	17.8 (23.0)
SE	0.89 (0.64)	6.0 (68.5)	15.7 (179.0)	12.2 (73.8)	0.86 (0.54)	5.7 (74.6)	11.6 (153.6)	14.2 (81.6)
SW	0.75 (0.05)	1.2 (54.4)	3.1 (141.5)	9.1 (63.1)	0.70 (-0.08)	-1.6 (53.4)	-3.1 (102.6)	12.6 (65.9)
NW	0.74 (0.32)	4.9 (-62.3)	5.3 (-67.7)	32.2 (71.1)	0.63 (0.32)	3.9 (-84.3)	3.3 (-70.8)	42.4 (94.6)
Central	0.90 (0.70)	-2.7 (12.6)	-3.9 (18.3)	13.2 (27.9)	0.83 (0.41)	-7.3 (-4.6)	-7.5 (-4.7)	20.6 (39.2)
	NO_2 ($\mu g/m^3$)				SO_2 ($\mu g/m^3$)			
	R	MBE	NMB(%)	RMSE	R	MBE	NMB (%)	RMSE
NCP	0.94 (0.62)	1.7 (7.6)	5.3 (24.2)	5.9 (14.6)	0.79 (0.60)	0.0 (57.1)	0.4 (455.4)	2.8 (63.3)
NE	0.91 (0.55)	1.4 (-0.2)	5.1 (-0.7)	5.7 (10.6)	0.71 (0.54)	1.1 (32.8)	6.2 (187.8)	4.6 (36.1)
SE	0.91 (0.49)	0.6 (9.5)	2.7 (45.5)	5.1 (13.3)	0.61 (0.35)	-0.6 (42.5)	-9.5 (680.1)	1.2 (44.7)
SW	0.76 (0.23)	0.0 (-2.0)	0.0 (-10.6)	6.1 (8.8)	0.51 (0.16)	-0.5 (42.4)	-6.7 (565.8)	1.7 (45.5)
NW	0.78 (0.27)	-4.9 (-22.3)	-12.6 (-57.3)	12.3 (28.3)	0.23 (-0.02)	-1.2 (13.5)	-8.2 (88.7)	5.6 (17.9)
Central	0.90 (0.57)	-2.0 (-6.1)	-6.5 (-20.0)	6.5 (13.1)	0.73 (0.54)	-1.3 (53.0)	-6.5 (270.9)	4.9 (58.6)
	CO (mg/m^3)				O_3 ($\mu g/m^3$)			
	R	MBE	NMB(%)	RMSE	R	MBE	NMB (%)	RMSE
NCP	0.92 (0.85)	-0.03 (0.08)	-2.2 (7.5)	0.16 (0.23)	0.78 (0.61)	-14.5 (-28.8)	-28.6 (-56.9)	20.7 (33.1)
NE	0.92 (0.78)	0.05 (-0.33)	5.4 (-34.5)	0.15 (0.43)	0.64 (0.58)	-17.7 (-25.3)	-32.7 (-46.7)	22.7 (28.5)
SE	0.83 (0.74)	-0.05 (0.11)	-6.0 (13.9)	0.10 (0.19)	0.79 (0.74)	-7.2 (-18.2)	-14.0 (-35.6)	15.8 (22.3)
SW	0.63 (0.62)	-0.08 (-0.02)	-10.0 (-1.9)	0.17 (0.18)	0.83 (0.82)	-5.7 (3.0)	-11.8 (6.2)	11.7 (10.5)
NW	0.70 (0.08)	0.11 (-1.13)	7.6 (-76.3)	0.46 (1.26)	0.66 (0.38)	-18.9 (-4.7)	-37.6 (-9.3)	25.4 (21.4)
Central	0.91 (0.76)	-0.08 (-0.37)	-7.5 (-33.5)	0.18 (0.43)	0.74 (0.70)	-17.9 (-14.8)	-35.3 (-29.3)	23.7 (22.2)

Table S2. The time of degrading responses level to COVID-19 virus in each province of mainland China.

Province	Region	date	Measurement
Beijing	NCP	30th Apr 2020	Degrade first level of response to second level
Tianjin	NCP	30th Apr 2020	Degrade first level of response to second level
Hebei	NCP	30th Apr 2020	Degrade first level of response to second level
Henan	NCP	19th Mar 2020	Degrade first level of response to second level
Shandong	NCP	7th Mar 2020	Degrade first level of response to second level
Inner Mongolia	NE	25th Feb 2020	Degrade first level of response to third level
Jilin	NE	26th Feb 2020	Degrade first level of response to second level
Liaoning	NE	4th Mar 2020	Degrade first level of response to second level
Shanghai	SE	24th Mar 2020	Degrade first level of response to second level
Anhui	SE	25th Feb 2020	Degrade first level of response to second level
Guangdong	SE	24th Feb 2020	Degrade first level of response to second level
Guangxi	SE	24th Feb 2020	Degrade first level of response to third level
Jiangsu	SE	25th Feb 2020	Degrade first level of response to second level
Jiangxi	SE	12th Mar 2020	Degrade first level of response to second level
Zhejiang	SE	2nd Mar 2020	Degrade first level of response to second level
Hainan	SE	26th Feb 2020	Degrade first level of response to third level
Hubei	SE	2nd May 2020	Degrade first level of response to second level
Hunan	SE	10th Mar 2020	Degrade first level of response to second level
Fujian	SE	27th Feb 2020	Degrade first level of response to second level
Yunnan	SW	24th Feb 2020	Degrade first level of response to third level
Sichuan	SW	26th Feb 2020	Degrade first level of response to second level
Guizhou	SW	24th Feb 2020	Degrade first level of response to third level
Chongqing	SW	10th Mar 2020	Degrade first level of response to second level
Xizang	SW	7th Mar 2020	Degrade first level of response to third level
Ningxia	Central	28th Feb 2020	Degrade first level of response to second level
Shanxi	Central	24th Feb 2020	Degrade first level of response to second level
Gansu	Central	21st Feb 2020	Degrade first level of response to third level
Shanaxi	Central	28th Feb 2020	Degrade first level of response to third level
Qinghai	Central	26th Feb 2020	Degrade first level of response to third level
Xinjiang	NW	26th Feb 2020	Degrade first level of response to second level

Table S3. Inversion estimated emissions of different air pollutants in southeast China as well as their changes between different periods in COVID-19 time

	NO_x	$PM_{2.5}$	PM_{10}	SO_2	CO
P1 (Gg/day)	57.1	34.8	60.9	17.9	876.3
P2 (Gg/day)	32.9	31.8	52.1	16.0	774.7
P3 (Gg/day)	35.9	34.3	71.0	17.0	805.2
(P2-P1)/P1	-42.4%	-8.6%	-14.3%	-10.9%	-11.6%
(P3-P2)/P1	5.2%	7.2%	31.0%	5.7%	3.5%
(P3-P1)/P1	-37.2%	-1.4%	16.6%	-5.2%	-8.1%

Table S4: Evaluation statistics for the meteorology simulation

Region	U (m/s)			V (m/s)			T (℃)			RH (%)			Precipitation (mm/day)		
	R	MBE	RMSE	R	MBE	RMSE	R	MBE	RMSE	R	MBE	RMSE	R	MBE	RMSE
NCP	0.92	-0.04	0.72	0.96	-0.38	1.31	0.98	-0.71	1.07	0.91	-7.95	9.76	0.88	0.06	1.22
NE	0.90	0.35	0.51	0.97	-0.45	1.01	0.98	-3.13	3.25	0.79	6.53	7.47	0.95	0.20	0.36
SE	0.95	-0.32	0.69	0.96	-0.55	1.07	0.99	-0.21	0.58	0.96	-5.44	6.80	0.91	0.59	1.96
SW	0.46	0.00	0.78	0.65	0.24	1.48	0.96	-0.19	0.81	0.81	-8.53	9.66	0.56	0.42	2.38
NW	-0.01	-0.39	1.27	0.16	0.16	0.64	0.96	2.07	2.60	0.94	4.71	6.23	0.86	0.01	0.08
CENTRAL	0.92	-0.04	0.72	0.78	-0.26	0.60	0.94	-0.73	1.42	0.88	-0.40	6.14	0.91	0.26	0.53

References:

Dunlea, E. J., Herndon, S. C., Nelson, D. D., Volkamer, R. M., San Martini, F., Sheehy, P. M., Zahniser, M. S., Shorter, J. H., Wormhoudt, J. C., Lamb, B. K., Allwine, E. J., Gaffney, J. S., Marley, N. A., Grutter, M., Marquez, C., Blanco, S., Cardenas, B., Retama, A., Villegas, C. R. R., Kolb, C. E., Molina, L. T., and Molina, M. J.: Evaluation of nitrogen dioxide chemiluminescence monitors in a polluted urban environment, Atmos. Chem. Phys., 7, 2691-2704, https://doi.org/10.5194/acp-7-2691-2007, 2007.

Lamsal, L. N., Martin, R. V., van Donkelaar, A., Steinbacher, M., Celarier, E. A., Bucsela, E., Dunlea, E. J., and Pinto, J. P.: Ground-level nitrogen dioxide concentrations inferred from the satellite-borne Ozone Monitoring Instrument, J. Geophys. Res.-Atmos., 113, https://doi.org/10.1029/2007JD009235, 2008.